

Accepted Manuscript

Capsaicin-like analogue induced selective apoptosis in A2058 melanoma cells:
Design, synthesis and molecular modeling

Gustavo José Vasco Pereira, Maurício Temotheo Tavares, Ricardo Alexandre Azevedo, Barbara Behr Martins, Micael Rodrigues Cunha, Rajesh Bhardwaj, Yara Cury, Vanessa Olzon Zambelli, Euzébio Guimarães Barbosa, Matthias A. Hediger, Roberto Parise-Filho

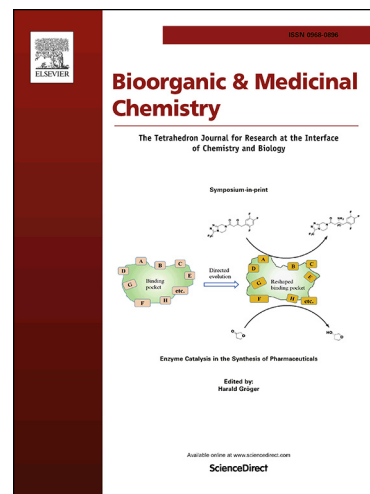
PII: S0968-0896(19)30087-2
DOI: <https://doi.org/10.1016/j.bmc.2019.05.020>
Reference: BMC 14907

To appear in: *Bioorganic & Medicinal Chemistry*

Received Date: 16 January 2019
Revised Date: 13 April 2019
Accepted Date: 12 May 2019

Please cite this article as: Pereira, G.J.V., Tavares, M.T., Azevedo, R.A., Martins, B.B., Cunha, M.R., Bhardwaj, R., Cury, Y., Zambelli, V.O., Barbosa, E.G., Hediger, M.A., Parise-Filho, R., Capsaicin-like analogue induced selective apoptosis in A2058 melanoma cells: Design, synthesis and molecular modeling, *Bioorganic & Medicinal Chemistry* (2019), doi: <https://doi.org/10.1016/j.bmc.2019.05.020>

This is a PDF file of an unedited manuscript that has been accepted for publication. As a service to our customers we are providing this early version of the manuscript. The manuscript will undergo copyediting, typesetting, and review of the resulting proof before it is published in its final form. Please note that during the production process errors may be discovered which could affect the content, and all legal disclaimers that apply to the journal pertain.



Capsaicin-like analogue induced selective apoptosis in A2058 melanoma cells: Design, synthesis and molecular modeling

Gustavo José Vasco Pereira,^{a†} Maurício Temotheo Tavares,^{a†} Ricardo Alexandre Azevedo,^b Barbara Behr Martins,^c Micael Rodrigues Cunha,^{a,d} Rajesh Bhardwaj,^e Yara Cury,^c Vanessa Olzon Zambelli,^c Euzébio Guimarães Barbosa,^f Matthias A. Hediger,^e Roberto Parise-Filho^{a*}

^aLaboratory of Design and Synthesis of Bioactive Substances (LAPSSB). Department of Pharmacy. Faculty of Pharmaceutical Sciences. University of São Paulo. São Paulo. Brazil.

^bExperimental Oncology Unit (UNONEX). Department of Microbiology, Immunology and Parasitology. Federal University of São Paulo. São Paulo. Brazil

^cLaboratory of Pain and Signaling. Butantan Institute. São Paulo. Brazil

^dDepartment of Chemistry and Biochemistry, University of Bern, Freiestrasse 3, 3012 Bern

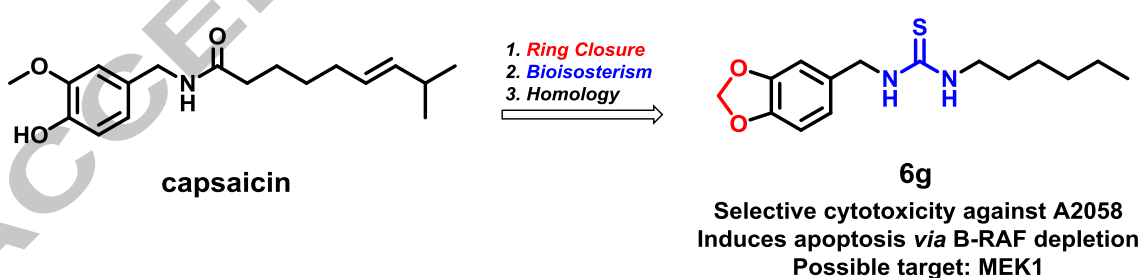
^eInstitute of Biochemistry and Molecular Medicine, National Center for Competence in Research, NCCR TransCure, University of Bern, Bühlstrasse 28, 3012 Bern.

^fDepartment of Pharmacy. Federal University of Rio Grande do Norte. Natal. Brazil

[†]These authors contributed equally for this work.

*Corresponding Author: R.P. E-mail: roberto.parise@usp.br

Graphical Abstract



Abstract

The use of molecules inspired by natural scaffolds has proven to be a very promising and efficient method of drug discovery. In this work, capsaicin, a natural product from *Capsicum* peppers with antitumor properties, was used as a prototype to obtain urea and thiourea analogues. Among the most promising compounds, the thiourea compound **6g**

exhibited significant cytotoxic activity against human melanoma A2058 cells that was twice as high as that of capsaicin. Compound **6g** induced significant and dose-dependent G₀/G₁ cell cycle arrest in A2058 cells triggering cell death by apoptosis. Our results suggest that **6g** modulates the RAF/MEK/ERK pathway, inducing important morphological changes, such as formation of apoptotic bodies and increased levels of cleaved caspase-3. Compared to capsaicin, **6g** had no significant TRPV1/6 agonist effect either irritant effects on mice. Molecular modeling studies corroborate the biological findings and suggest that **6g**, besides being a more reactive molecule towards its target, may also present a better pharmacokinetic profile than capsaicin. Inverse virtual screening strategy found MEK1 as a possible biological target for **6g**. Consistent with these findings, our observations suggested that **6g** could be developed as a potential anticancer agent.

Keywords: peppers; anticancer agents; drug design; natural product; capsaicin; urea; thiourea; cancer; chemotherapy; apoptosis.

Introduction

The term "cancer" is used to describe a set of changes that shares the common characteristic of uncontrolled cell growth.¹ In 2012, 14.1 million cases of cancer were estimated around the world, where the expectation for 2035 could reach 24 million cases.² Thus, cancer is the second largest cause of death worldwide.² Although there are strategic therapies for the treatment of cancer, low selectivity to tumorigenic cells, high toxicity, resistance and high cost are persistent issues in this field.^{3,4} In view of this, natural products have played an important role for the design of new drugs, offering active substances to various diseases.⁵ Capsaicin (Fig. 1A) is abundantly found in *Capsicum* peppers and it is a secondary metabolite derived from the condensation of vanillylamine with (*E*)-8-methylnon-6-enoic acid. A large number of independent studies demonstrates the ability of capsaicin to prevent both mutagenic and carcinogenic processes *in vitro* and *in vivo*.^{11–15} Moreover, several biological properties including agonist effects over TRPV1 receptors are reported.^{6–10}

According to Walpole and coworkers the structure of capsaicin can be divided in three main regions.^{16–18} The A-region consists in the vanillyl moiety;¹⁶ the B-region presents the secondary amide linker that connects both extremes of the molecule;¹⁷ and C-region comprises an unsaturated hydrophobic tail derived from the fatty acid.¹⁸ Several structure-activity relationship (SAR) studies were carried out regarding the design of TRPV1 agonists and antagonists, through systematic changes over the A-, B-, and C-region of capsaicin.^{19–21} Noteworthy, unsaturation of C-region has no significant influence in the potency of capsaicin-like compounds, which could be observed for – but not only – dihydrocapsaicin who promotes equipotent cellular Ca^{2+} influx (via TRPV1), and consequently similar pungency as capsaicin.^{21,22}

Regarding the antitumor mechanism of capsaicin, this remains to be elucidated,^{23–26} although several studies suggest that this effect may be the result of the activation of two signaling pathways: i) the intrinsic or mitochondrial pathway, with late activation of caspase 1 and 3; and ii) the extrinsic or receptor-dependent pathway, through capsaicin action on TRPV-like channels.²⁷ Our group has developed several analogues of capsaicin that presented selective cytotoxicity for several breast, skin, and lung tumorigenic cell lines.^{28–31} Thus, we have concentrated our recent efforts on the production of new series of capsaicin analogues (Fig. 1B). The series were designed by keeping the same vanillyl moiety of capsaicin in A-region and also by its ring closure, generating the 1,3-benzodioxole bicyclic system (Fig. 1B) which is commonly found in

antineoplastic agents such as podophyllotoxin, etoposide and derivatives. The amide linker in B-region suffered bioisosteric replacements, generating the urea and thiourea series. In addition, the lipophilic tail of capsaicin in the C-region has been replaced by alkyl and aryl substituents, conserving the hydrophobic character of this region for the compounds. Herein, we describe the design and synthesis of two series of ureidic and thioureidic analogues quite similar to capsaicin. The biological activities and anticancer mechanism of these compounds were investigated. *In silico* studies were also performed to provide information about SAR.

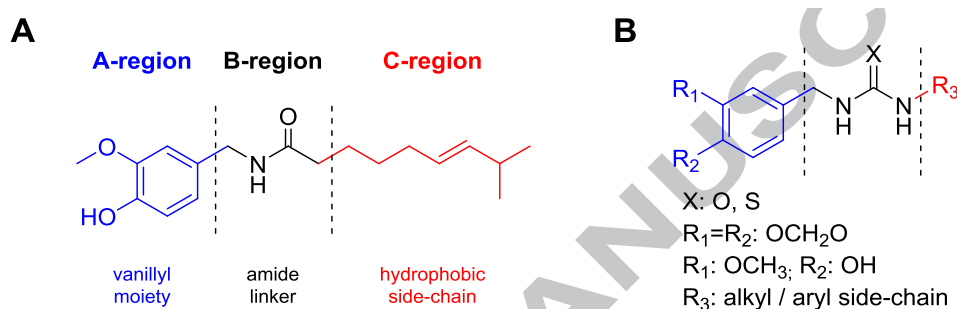
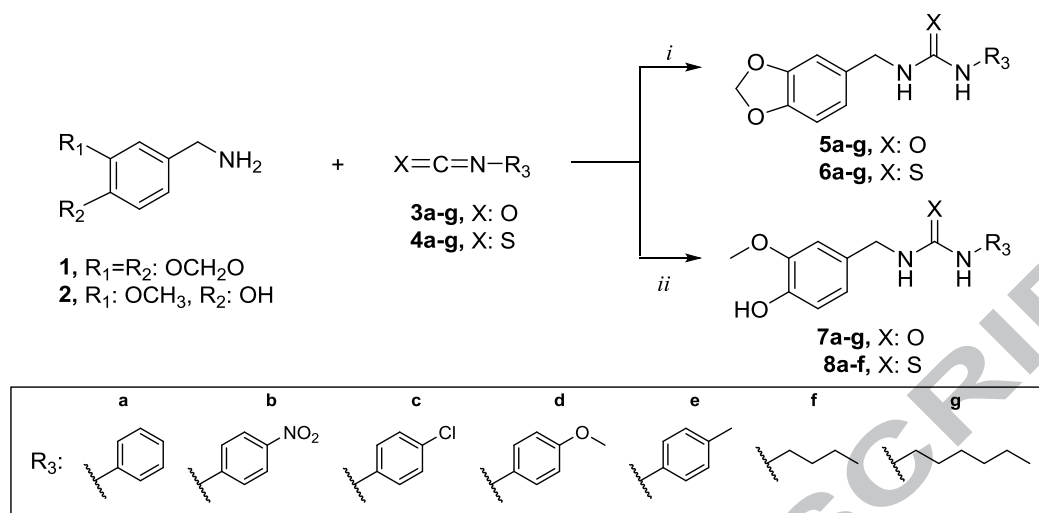


Fig. 1. (A) Chemical structure of capsaicin. (B) General structure of the designed analogues of this work.

Results and discussion

Chemistry

The method applied for the synthesis of the capsaicinoid derivatives was the nucleophilic addition of primary amines to the carbonyl or thiocarbonyl, thus generating ureidic and thioureidic derivatives. The final products were synthesized in a single step by the reaction of piperonylamine (**1**) or vanillylamine (**2**) with isocyanates (**3a-3g**) or isothiocyanates (**4a-4g**) as shown in Scheme 1. Twenty-seven analogues were synthesized and characterized by ¹H and ¹³C NMR, melting range, and the purity was determined by HPLC. All compounds showed a solid appearance, with yields ranging from 22 to 90%.

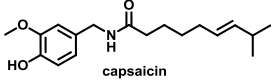
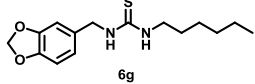
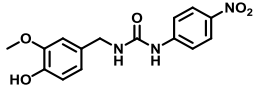
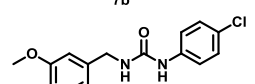
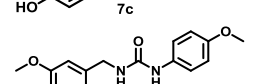


Scheme 1. Synthesis of piperonyl (**5a-g**; **6a-g**) and vanillyl (**7a-g**; **8a-f**) analogues. Reagents and conditions: i) CH_2Cl_2 , cat. Et_3N , atm. N_2 , r.t., 3 h; ii) $CH_2Cl_2/MeOH$ (8:2), cat. Et_3N , atm. N_2 , r.t., 4 h.

Cell viability assay and morphological evaluation

The cytotoxicity of all compounds (**5a-g**, **6a-g**, **7a-g** and **8a-f**) were evaluated by the MTT assay against a panel of tumorigenic cell lines including B16F10 (murine melanoma), A2058 and SK-MEL-25 (human melanoma), MCF-7 (human breast adenocarcinoma), HeLa (cervical carcinoma) and U-87 (glioblastoma). Furthermore, we also tested the compounds against non-tumorigenic human fibroblasts (T75) cells to verify the selectivity index (SI) of the compounds. Our results showed that compounds (**6g**, **7b-d**) showed superior cytotoxic activity compared to the prototype against human melanoma tumor cells A2058 and SK-MEL-25, as well as human glioblastoma U-87, with an effectiveness ranging from 55.17 μM to 98.7 μM (Table 1). On the other hand, they were not able to replicate the same effect over MCF-7 breast adenocarcinoma, human cervical adenocarcinoma HeLa (data not shown) and murine B16F10 melanoma cells. Particularly, compound **6g** showed pronounced activity with IC_{50} values of 55, 67, and 87 μM against A2058, SK-MEL-25, and U-87 cells, respectively, which represent one- to two-fold improvement in potency compared to capsaicin. Noteworthy, compound **6g** presented the highest SI for A2058 (SI: 1.8, Table 1).

Table 1. Biological data for compounds **6g**, **7b-d**.

Compounds	IC ₅₀ (μM) ± SD ^e					SI [‡]
	SK-MEL-25	A2058	U-87	B16F10	T75	
 capsaicin	>100	>100	>100	>100	>100	-
 6g	67.19 ± 8.7	55.17 ± 9.35	86.95 ± 7.44	>100	>100	>1.8
 7b	98.7 ± 7.35	98.20 ± 8.34	98.54 ± 8.55	>100	>100	>1.1
 7c	90.5 ± 6.97	84.45 ± 7.67	92.48 ± 7.98	>100	>100	>1.18
 7d	91.8 ± 7.45	92.54 ± 7.89	> 100	>100	>100	>1.08

^eData are expressed as means ± SD obtained from three independent experiments.[‡]SI: selectivity index, determined by the ratio between IC₅₀ A2058 e T75

As a tendency, the compounds were more effective in A2058 and SK-MEL-25 human melanoma cells, both having a mutation in the B-RAF protein (B-RAF^{V600E} mutation).^{32,33} Preliminarily, we suggest that this mutation can be considered a possible target of compound **6g**, thereby triggering cytotoxic activity. This hypothesis became more evident when compared to the effects found in B16F10 (wild-type B-RAF) strains,^{34–36} which only showed an antiproliferative effect with IC₅₀ higher than the highest concentration used in the initial screenings. This situation is particularly interesting since 50% of melanomas of all clinical types have B-RAF mutations.³⁷

Among the most active compounds, **6g** which has the 1,3-benzodioxole moiety at the A-region and bearing a *n*-alkyl side chain bound to the thiourea linker exhibited improved activity against A2058 cells relative to corresponding urea compounds **7b-d** bearing the bulky *para*-substituted benzyl group. Regarding urea analogues, those with electron-donating groups, (EDG) such as compounds **7c** and **7d**, appear to result in more active compounds, which may be due the increase in the electronic density of the aromatic ring. Compound **7b** corroborates this hypothesis, whereas its electron-withdrawing nitro group (EWG, NO₂), proved to be the least active analogue.

With these results, compound **6g** was chosen for further investigations regarding mechanistic studies of the cytotoxic effect. Our results confirm that **6g** affects the overall morphology of A2058 cells, disrupting the formation of structures that resemble the *in vivo* architecture of those cells. The morphology of A2058 melanoma cells treated with compound **6g** is presented in Fig. 2A. As observed in comparison to the control,

the changes induced by **6g** suggest cell death by apoptosis, since there is loss of cell adhesion, significant withdrawal of the cytoplasm, loss of refringence and marked formation of apoptotic bodies.^{38,39} Compared to the effects of **6g** on B16F10 melanoma cells (Fig. 2B), it is possible to observe that the cells are not dead, but there are, clearly, fewer cells-per-well, suggesting cell cycle arrest.

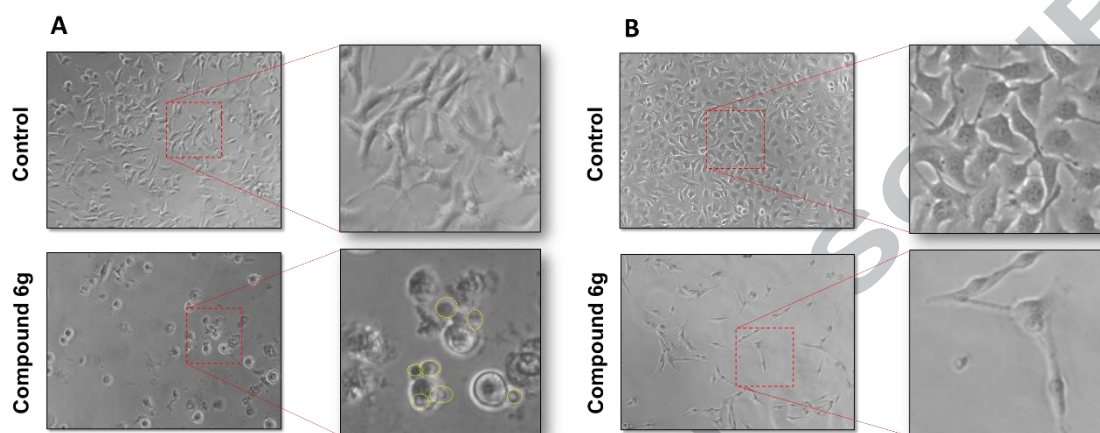


Fig. 2. (A) Photomicrographs show the morphological aspects of melanoma control cultures of A2058 cells (top), and treated with **6g** (bottom). (B) Morphological aspects of control cultures of B16F10 melanoma cells (top), and treated with **6g** (bottom). Cultures were incubated for 24 h at 37 °C. Yellow dashed circles indicate the appearance of apoptotic bodies. Grids (in red) indicate enlargement of the area.

Cell Cycle Analysis and Cell Death Studies

Analysis of the morphology of human A2058 and murine B16F10 melanoma cells provided evidence that there are distinct biological effects, particularly related to cell cycle arrest and possible death by apoptosis. To investigate effects on the cell cycle, cells were treated with compound **6g** at concentrations of 12.5, 25.0 and 50.0 μ M and then labeled with propidium iodide. The distribution of cell cycle phases was measured by flow cytometry. The data showed that compound **6g** at 50 μ M was able to increase the G_0/G_1 phase, suggesting an arrest at this stage of the cycle in murine B16F10 melanoma cells (Fig. 3A). As noted, this behavior has been shown to be dose-dependent. In addition, there is no variation in the sub G_0/G_1 population compared to the control (vehicle), indicating that there is no cell death.⁴⁰⁻⁴² On the other hand, A2058 human melanoma cells treated with compound **6g** have shown a significant shift of the cell population in sub G_0/G_1 , suggesting that those cells might be in the process of cell death (Fig. 3B). Noteworthy, compound **6g** induced a significant and dose-dependent G_0/G_1 cell cycle arrest in A2058 cells.⁴³

After obtaining evidence of the type of cell death involved in the effect triggered by compound **6g**, the next step was to characterize the cell death phenomenon by analyzing the levels of anti-apoptotic mediator (Bcl-xl) and effector caspase 3 in its active isoform (Casp3)⁴⁴⁻⁴⁶ by western blotting. It is important to note that capsaicin derivatives as dihydrocapsaicin may act as autophagy inducers⁴⁷ even though we did not observed any evidences of autophagic bodies in our preliminary studies.

As observed in Fig. 3C, our results clearly show the up-regulation effect of the active isoform of the pro-apoptotic protein and the downregulation of the antiapoptotic protein. After 1 h, there is a considerable reduction in B-RAF (ratio 1 to 0.45) indicating that the pathway is being modulated by compound **6g**. These data are corroborated by the abrupt reduction of C-RAF from 3 hours (1 to 0.49) of treatment.⁴⁸ Also in Fig. 3C, the 6-hour analysis reveals a reduction in the concentration of Bcl-xl antiapoptotic protein, as well as reduction of total caspase 3 and, consequently, increase of the active form Casp3. The involvement and increase of cleaved Casp3 corroborates our cellular morphology data and altogether indicate that cell death is by apoptosis, in a possible activation of the apoptotic RAF/MEK/ERK pathway.^{49,50}

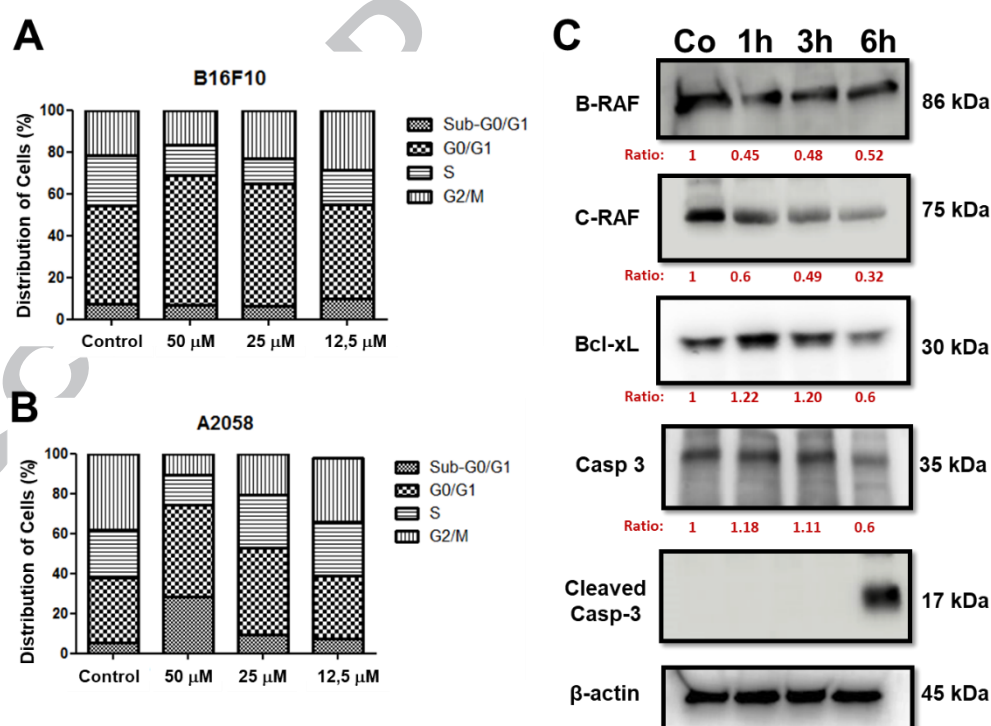


Fig. 3. (A) Distribution of the percentage of cell cycle phases in B16F10 cells treated with compound **6g**. (B) Distribution of cell cycle phases of A2058 cells treated with compound **6g**. (C) Western blotting of the A2058 cells treated with compound **6g**, demonstrating the increase levels of caspase 3 over time. Protein expression was quantified with ImageQuant LAS4000 software and normalized to β -actin expression.

Evaluation of TRPV1 activity

After this preliminary screening, our next goal was to test the effect of **6g** on the activity of human TRPV1⁵¹ transiently expressed in HEK293T cells, in order to collect data that point out toward a more detailed mechanistic explanation.^{52,53}

Capsaicin was selected as standard TRPV1 activator and was used to develop the protocol. For screening of compounds with antagonist activity, capsazepine was selected as internal positive control. In our hands, capsaicin evoked an increase in Ca^{2+} transport through TRPV1, with an EC_{50} of 7.2 ± 4.1 nM,⁵⁴ whereas the non-transfected cells (HEK_nT) showed no transport (supplementary material - Fig. S1A and S1B). Therefore, 100 nM capsaicin was sufficient to stimulate the channel to its maximum. The antagonist of TRPV1, capsazepine, was found to inhibit the 100 nM capsaicin-mediated activation of TRPV1, with an IC_{50} of 174.1 nM^{55,56} (supplementary material - Fig. S1C).

Compound **6g** profoundly evoked the influx of Ca^{2+} through TRPV1 in HEK293T cells transiently transfected with TRPV1, but only marginally in untransfected cells (Fig. S1D), suggesting that **6g** acts as an agonist. However, the activity was nearly 640-fold lower than that of capsaicin, with EC_{50} of 4.62 ± 0.08 μM (Fig. 4A). To validate the agonist effects of **6g**, we pretreated the cells with vehicle (DMSO, 0.1% in buffer) or capsazepine (10 μM). Remarkably, both, the activity of capsaicin (100 nM) and **6g** (10 μM) were completely abolished by the pretreatment with capsazepine (10 μM) (Fig. 4B).⁵⁷ To evaluate, whether the human epithelial calcium channel TRPV6 can be targeted by **6g**, we tested the effect of **6g** and also capsaicin on the activity of the TRPV6 channel stably expressed in HEK293 cells.⁵⁸ Fig. 4C indicates that **6g** at 50 μM , as well as capsaicin at 100 nM, showed no discernable effect on TRPV6 activity, indicating that these compounds possess selectivity toward TRPV1, whereas the previously published inhibitor *cis*-22a⁵⁹ effectively blocked TRPV6 at 2.5 μM (Fig. 4C).

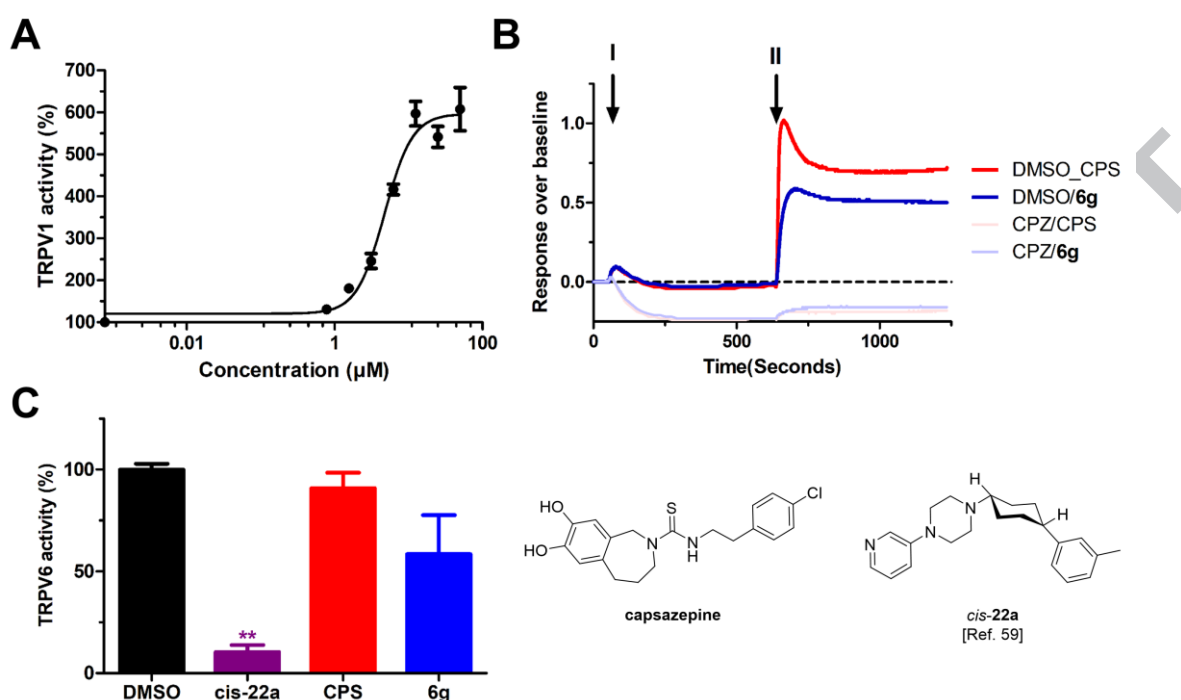


Fig. 4. (A) Dose-response curve of **6g** in HEK_TRPV1 cells. Data shown is mean \pm SEM (n = 6/concentration). (B) Ca²⁺ traces of HEK_TRPV1 cells. I = first application (DMSO or capsazepine – CPZ – 10 μ M). II = second application (capsaicin – CPS – 100 nM or **6g**, 10 μ M). (C) Evaluation of the capsaicin (CPS) and **6g** in HEK-TRPV6 cells. Data shown is mean \pm SEM (n = 3/concentration). Significance between the treated groups was determined by one-way ANOVA and Tukey test. **p < 0.01 (by comparison with vehicle).

Evaluation of nociceptive potential of **6g** compared to capsaicin

TRPV1 plays a key role in the development of various pathological processes, most prominently in the sensations of heat and inflammation, and mediates the pungency and pain sensations associated with capsaicin.^{52,60–63} In order to verify whether – *in vivo* – the compound **6g** has the ability to activate TRPV1 channel in a similar way as capsaicin, the flinching behavior was assessed.⁵³ The test measured the number of flinches during 5 minutes and indicates nociceptive intensity after intraplantar application of 20 μ L of vehicle (EtOH + saline), capsaicin and **6g** – both at 0.26 M concentration (5.2 nmol/paw). Results are presented in Fig. 5.

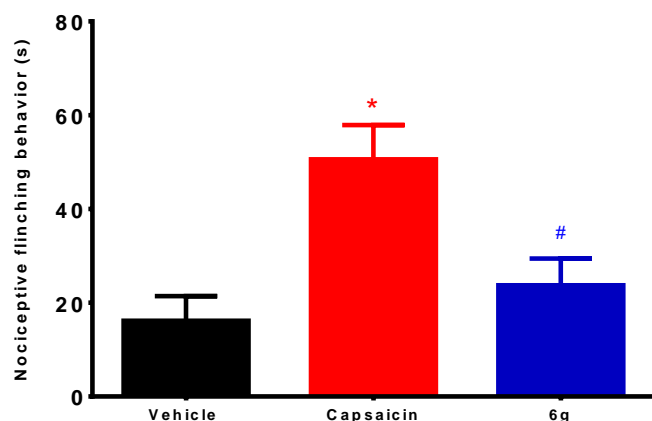


Fig. 5. Evaluation of the capsaicin and **6g** effect on the nociceptive behavior of mice. All animals received the vehicle and tested compounds by intraplantar route (5.2 nmol/paw, 20 μ L of a 0.26 M solution). $n = 8$ animals. Significance between the treated groups was determined by one-way ANOVA and Tukey test. * $p < 0.05$ (by comparison with vehicle); # $p < 0.05$ (by comparison with capsaicin).

As can be seen, capsaicin injection evoked nociceptive response when compared to the vehicle. On the other hand, the compound **6g** injection generated significantly lower effect in treated animals, indicating that this compound is less effective to induce nociceptive behavior as compared to capsaicin. These results suggest that **6g** may not be acting exclusively *via* TRPV1 receptor activation. Therefore, the more pronounced antitumor effect compared to capsaicin is probably due to the action over other receptor subtypes or, corroborating the data found in this work, the action may be due to modulation of the RAF/MEK/ERK pathway. However, given that the potency of **6g** to activate TRPV1 is substantially lower than that of capsaicin, it seems unlikely that the phenotype exhibited by **6g** treated mice is related to activation of TRPV1.

Molecular modeling

The purpose of the theoretical approach was to find energetically more favorable conformations of capsaicin and **6g**, and thus to calculate molecular properties with purpose of providing ideas about structure-activity relationships (SAR).⁶⁴ The calculation of the properties was performed in the Spartan'14 program, obtaining: electrostatic potential map (MPE), energy of the HOMO and LUMO (E_{HOMO} and E_{LUMO}) frontier orbitals, partition coefficient (ClogP), hydrogen bond acceptor site (HBA), hydrogen bonding donor site (HBD), polar surface area (PSA), and dipole moment (μ).

Table 2 shows the calculated values for the molecular properties of capsaicin and compound **6g**. According to the calculated values of ClogP, 3.66 for capsaicin and 3.92 for compound **6g**, the molecules have similar hydrophobic character, although the latter is slightly more lipophilic. In addition, PSA (48.21 Å² and 36.60 Å² for capsaicin and **6g**, respectively) showed that compound **6g** presents the lower surface of all polar atoms, corroborating its greater hydrophobicity. These data together indicate that the more hydrophobic profile of **6g** may result in higher cell membrane permeability, suggesting the better activity of the compound compared to capsaicin.⁶⁵ Regarding HBD, HBA and MW properties, all have values that follow drug-like rules.⁶⁶

Table 2. Calculated molecular properties for capsaicin and **6g**.

Molecular Properties	capsaicin	6g
ClogP	3.66	3.92
E _{HOMO} (eV)	-8.27	-8.51
E _{LUMO} (eV)	3.98	3.70
Gap = E _{HOMO} - E _{LUMO}	-12.25	-12.21
μ Debye (D)	3.96	7.57
PSA (Å ²)	48.21	36.60
HBA	4	5
HBD	2	2

The energy values of the frontier molecular orbitals (E_{HOMO} e E_{LUMO}), as well as the difference between them (Gap = E_{HOMO} - E_{LUMO}), were calculated from the lower energy conformational models of capsaicin and compound **6g**. The values are described in Table 2 and the HOMO and LUMO maps are shown in Fig. 6A. Although the calculated energy values are quite similar, **6g** has a lower E_{LUMO} (3.70 eV) than capsaicin (E_{LUMO} = 3.94 eV), characterizing it as being a more electron accepting molecule. LUMO map distributions did not show significant differences between the two investigated molecules.²⁸

Regarding E_{HOMO} energy values, **6g** presents a slightly higher value when compared to the prototype. In addition, the HOMO map distribution shows a greater intensity of the HOMO orbital in the region where the bioisosteric replacement was performed (replacing the amide function by thiourea). The gap values (see Table 2) point out the benzodioxole derivative as a slightly more reactive molecule than capsaicin.

The dipole moment vector (μ) can be visualized as yellow arrows in Fig. 6B and the μ values are listed in Table 2. The dipole moment vector is defined as the total product of the amount of positive or negative charge and the distance between its centroids. As seen in Fig. 6B, the vectors are in opposite sides of the two molecules.

Moreover, the difference of the values of dipole moment between the molecules is given by the high electronic density of the thiourea moiety.⁶⁵ Regarding the electrostatic potential map (EPM, Fig. 6C), there is a higher electron density at the thiourea linker, which may be an additional data to understand the reasons why **6g** is more active than the prototype.⁶⁷

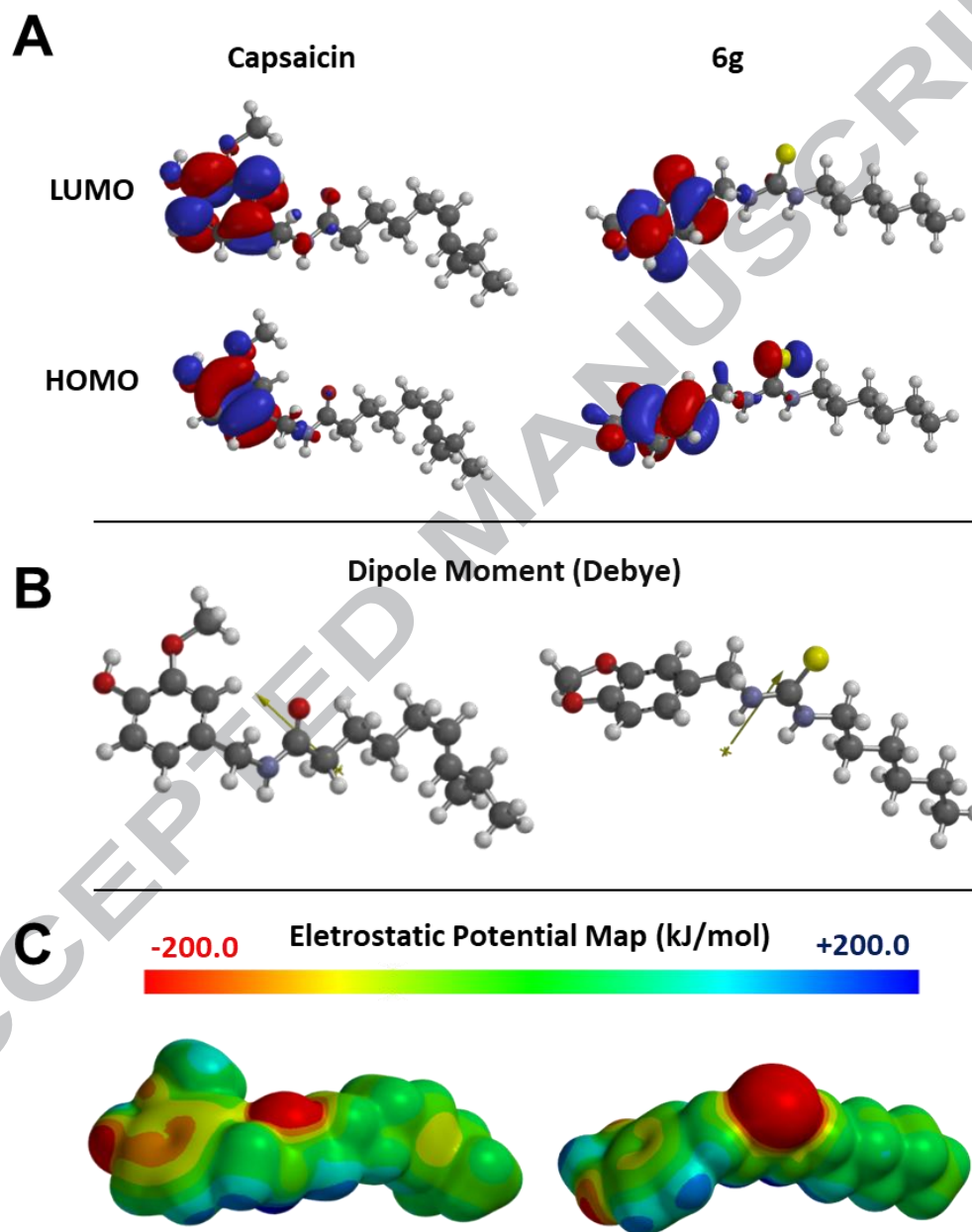


Fig.6. Electronic properties found for capsaicin and **6g**. (A) Distribution of molecular orbital maps, HOMO and LUMO (color range: -0.020 (red) to 0.020 (blue)). (B) Total dipole moment vector (yellow arrows), and (C) Electrostatic potential maps (EPMs; color range: -200.0 (intense red) to 200.0 (intense blue)). The molecules are presented as ball-wire models (carbon in gray, oxygen in red, nitrogen in blue, and hydrogen in white).

Regarding E_{HOMO} energy values, **6g** presents a slightly higher value when compared to the prototype. In addition, the HOMO map distribution shows a greater intensity of the HOMO orbital in the region where the bioisosteric replacement was performed (replacing the amide function by thiourea). The gap values (see Table 2) point out the benzodioxole derivative as a slightly more reactive molecule than capsaicin.

Inverse Virtual Screening and docking

The purpose of the inversed virtual screening was to find possible targets for the compound **6g**. In order to do so, a simplified version of **6g** was created by removing the long aliphatic chain attached to the thiourea moiety (**6g_mod**). The structure **6g_mod** was screened against all the PDB databank by ligand-based similarity search. Table 3 shows the entire cancer-related targets which the ligand has the highest similarities to compound **6g_mod**.

Table 3. Most promising targets for **6g** as pointed out by the ligand-based inversed virtual screening.

Target (PDB ID)	Ligand ID	Similarity
Proto-oncogene serine/threonine-protein kinase Pim-1 (5N4U)	8MZ	0.916
Mitogen-activated protein kinase kinase) MEK1 (5BX0)	4W5	0.910
Cyclin-dependent kinase 2 (2EXM)	ZIP	0.906
Phosphoinositide-Dependent Kinase-1 (PDK1) (3QCQ)	3Q0	0.887

The mitogen/extracellular signal-regulated kinase (MEK1) from the MAPK signaling cascade seems to be the best target among all. MEK1 regulates proliferation and other cellular processes by the phosphorylation and activation of downstream ERK proteins. These findings further corroborate the cell death study which the involvement and increase of cleaved Casp3 trigger apoptosis in a possible activation of the apoptotic RAF/MEK/ERK pathway. Fig. 7 shows a possible binding mode for **6g_mod** and MEK1 (PDB entry 5bx0).⁶⁸ The interaction is quite similar to the bound ligand (BL)

indazole in the hydrophobic pocket. Another important feature is that the pointed-out dipole moment vector created by the thiourea moiety points favorably to Gln153 forming a hydrogen bond like dipole-dipole interaction.

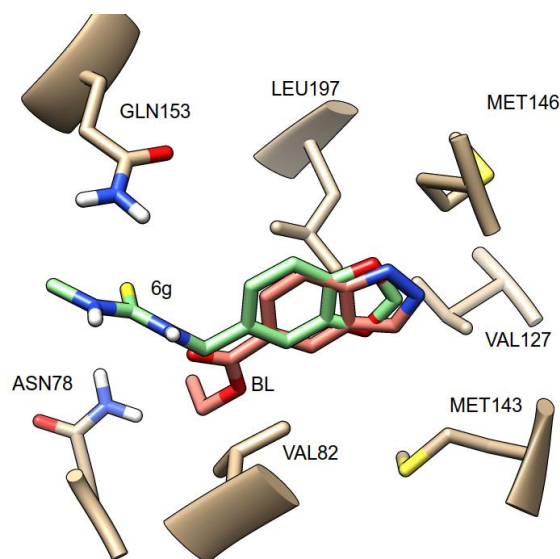


Fig. 7. Molecular docking pose of **6g_mod** bound to MEK1 cancer target. BL and **6g_mod** bind similarly by the alignment of the fused rings differing only the side chain interactions.

Conclusion

In conclusion, we show that the capsaicin-like analogue **6g** has a higher antitumor activity than its prototype – capsaicin – by inducing significant and dose-dependent G₀/G₁ cell cycle arrest in A2058 cells, which was associated with cellular morphological changes, indicating cell death by apoptosis. In addition, it is suggested that **6g** acts by modulating the RAF/MEK/ERK pathway and exhibited insignificant effects on TRPV-type vanilloid receptors. Molecular modeling studies suggest that **6g** is a more reactive molecule and may also present a better pharmacokinetic profile when compared to capsaicin. The inverse virtual screening strategy identified MEK1 as a promising target for compound **6g**. In summary, our observations suggested that compound **6g** could be developed as a potential anticancer agent.

Experimental

Chemistry

Reagents and solvents were purchased from Sigma-Aldrich, and were used without further purification. The following reagents were used to synthesize capsaicinoid derivatives: piperonylamine, vanilylamine, phenyl isocyanate, 4-

nitrophenyl isocyanate, 4-chlorophenyl isocyanate, 4-methoxyphenyl isocyanate, 4-tolyl isocyanate, butyl isocyanate, hexyl isocyanate, phenyl isothiocyanate, 4-nitrophenyl isothiocyanate, 4-chlorophenyl isothiocyanate, 4-methoxyphenyl isothiocyanate, 4-tolyl isothiocyanate, butyl isothiocyanate, hexyl isothiocyanate.

The melting points were measured by the Büchi M-565 apparatus. TLC was performed on silica gel plates (60 F₂₅₄ TLC, Merck Darmstadt, Germany) for monitoring the reaction and checking for impurity traces. Plate readings were performed under UV light at 254 nm. Flash chromatography was used in the purification of the compounds. ¹H and ¹³C nuclear magnetic resonance (NMR) spectra were recorded using a Bruker Advanced DPX-300 spectrometer at 300 MHz and 75 MHz, respectively. Chemical shifts were expressed as δ units, using tetramethylsilane (TMS) or solvent residual peak as internal standard. The spectral splitting patterns are described as follows: s, singlet; bs, broad singlet; d, doublet; dd, double doublet; q, quartet; t, triplet; m, multiplet peak. The chromatographic purity of the compounds was determined using a high performance liquid chromatograph (Shimadzu®-PROMINENCE) coupled to a C18 column (Shimadzu®-Shim-pack CLC-ODS 150 x 4.6 mm).

General procedure for the synthesis of compounds.

A) Synthesis of derivatives **5a-5g** and **6a-6g**:

Piperonylamine (1.1 mmol) and triethylamine (1 mmol) were diluted in 20 mL dichloromethane (DCM) in a 100 mL double neck round bottom flask coupled with an addition funnel of 50 mL. Isocyanate (1 mmol) or isothiocyanate (1 mmol) was dissolved in DCM (5 mL) and added dropwise to the solution of piperonylamine. The mixture was kept under stirring in nitrogen atmosphere for 3 hours. Then, the solvent was evaporated under reduced pressure and the product was purified by flash chromatography or recrystallization.

B) Synthesis of derivatives **7a-7g** e **8a-8f**:

Vanillylamine (1.1 mmol) and triethylamine (1 mmol) were diluted in 40 mL of dichloromethane:methanol (DCM:MeOH - 8:2) in a 100 mL double neck round bottom flask coupled with an addition funnel of 50 mL. Isocyanate (1 mmol) or isothiocyanate (1 mmol) was dissolved in DCM (5 mL) and added dropwise to the solution of

vanillylamine. The mixture was kept under stirring in nitrogen atmosphere for 4 hours. Then, the solvent was evaporated under reduced pressure and the product was purified by recrystallization.

1-(benzo[d][1,3]dioxol-5-ylmethyl)-3-phenylurea (5a):

White solid (Yield: 50%), m.p. 162–163.5 °C. ¹H NMR (DMSO-*d*₆, 300 MHz): 8.50 (s, 1H), 7.41 (d, *J* = 7.7 Hz, 2H), 7.23 (t, *J* = 7.3 Hz, 2H), 6.91 (d, *J* = 7.3 Hz, 1H), 6.87 (s, 1H), 6.85 (s, 1H), 6.79 (d, *J* = 8.0 Hz, 1H), 6.54 (t, *J* = 5.8 Hz, 1H), 5.98 (s, 2H), 4.21 (d, *J* = 5.9 Hz, 2H). ¹³C NMR (DMSO-*d*₆, 75 MHz): 155.2, 147.2, 146.0, 140.4, 134.2, 128.6, 121.1, 120.3, 117.7, 108.0, 107.8, 100.7, 42.5. HPLC analyses: 99.3%.

1-(benzo[d][1,3]dioxol-5-ylmetil)-3-(4-nitrophenil)urea (5b):

Yellow solid (Yield: 40%), m.p. 160.3–162.1 °C. ¹H NMR (DMSO-*d*₆, 300 MHz): 9.36 (s, 1H), 8.04 (bs, 1H), 7.96 (dd, *J*₁ = 9.0 Hz, *J*₂ = 3.1 Hz, 2H), 7.81 – 7.78 (m, 2H), 7.40 (s, 1H), 7.31 (d, *J* = 7.9 Hz, 1H), 7.23 (d, *J* = 7.9 Hz, 1H), 6.42 (s, 2H), 5.23 (d, *J* = 4.0 Hz, 2H). ¹³C NMR (DMSO-*d*₆, 75 MHz): 154.4, 147.2, 147.1, 146.1, 140.5, 133.7, 125.1, 120.4, 116.9, 108.0, 107.9, 100.8, 42.6. HPLC analyses: 95.4%.

1-(benzo[d][1,3]dioxol-5-ylmethyl)-3-(4-chlorophenyl)urea (5c):

White solid (Yield: 63%), m.p. 187.3–189.0 °C. ¹H NMR (DMSO-*d*₆, 300 MHz): 8.65 (s, 1H), 7.44 (d, *J* = 8.3 Hz, 2H), 7.26 (d, *J* = 8.3 Hz, 2H), 6.87 (s, 1H), 6.86 (d, *J* = 8.0 Hz, 1H), 6.78 (d, *J* = 7.9 Hz, 1H), 6.59 (t, *J* = 7.9 Hz, 1H), 5.48 (s, 2H), 4.21 (d, *J* = 4.2 Hz, 2H). ¹³C NMR (DMSO-*d*₆, 75 MHz): 155.0, 147.2, 146.0, 139.4, 134.1, 128.4, 124.5, 120.3, 119.2, 108.0, 107.8, 100.8, 42.6. HPLC analyses: 98.8%.

1-(benzo[d][1,3]dioxol-5-ylmethyl)-3-(4-methoxyphenyl)urea (5d):

White solid (Yield: 75%), m.p. 197.4–199.5 °C. ¹H NMR (DMSO-*d*₆, 300 MHz): 8.27 (s, 1H), 7.28 (d, *J* = 8.4 Hz, 2H), 6.86 (s, 1H), 6.84–6.75 (m, 4H), 6.41 (t, *J* = 5.9 Hz, 1H), 5.97 (s, 2H), 4.18 (d, *J* = 5.9 Hz, 2H), 3.69 (s, 3H). ¹³C NMR (DMSO-*d*₆, 75 MHz): 155.4, 154.0, 147.2, 145.9, 134.4, 133.5, 120.2, 119.5, 113.9, 108.0, 107.8, 100.7, 55.1, 42.6, 28.6. HPLC analyses: 97.6%.

1-(benzo[d][1,3]dioxol-5-ylmethyl)-3-(p-tolyl)urea (5e):

White solid (Yield: 90%;), m.p. 151.0–152.5 °C. ¹H NMR (DMSO-*d*₆, 300 MHz): 8.25 (s, 1H), 7.82 (d, *J* = 8.4 Hz, 2H), 7.49 (d, *J* = 8.3 Hz, 2H), 7.35 (s, 1H), 7.28 (d, *J* = 7.9 Hz, 1H), 7.23 (d, *J* = 7.3 Hz, 1H), 6.51 (bs, 1H), 6.41 (s, 2H), 4.77 (d, *J* = 5.8 Hz, 2H), 2.70 (s, 3H). ¹³C NMR (DMSO-*d*₆, 75 MHz): 155.3, 147.2, 146.0, 137.8, 134.3, 129.9, 129.0, 120.3, 117.8, 108.0, 107.8, 100.7, 42.5, 20.2. HPLC analyses: 99.4%.

1-(benzo[d][1,3]dioxol-5-ylmethyl)-3-butylurea (5f):

White solid (Yield: 75%), m.p. 197.0–198.5 °C. ¹H NMR (DMSO-*d*₆, 300 MHz): 6.83 (d, *J* = 7.9 Hz, 1H), 6.80 (s, 1H), 6.71 (d, *J* = 7.9 Hz, 1H), 6.19 (t, *J* = 5.7 Hz, 1H), 5.97 (s, 2H), 5.83 (t, *J* = 5.3 Hz, 1H), 4.10 (d, *J* = 6.0 Hz, 2H), 3.00 (q, *J* = 6.4 Hz, 2H), 1.38 – 1.23 (m, 4H), 0.87 (t, *J* = 7.1 Hz, 3H). ¹³C NMR (DMSO-*d*₆, 75 MHz):

155.3, 147.2, 146.0, 137.8, 134.3, 129.9, 129.0, 120.3, 117.8, 108.0, 107.8, 100.7, 42.5, 20.2. HPLC analyses: 97.6%.

1-(benzo[d][1,3]dioxol-5-ylmethyl)-3-hexylurea (5g):

White solid (Yield: 42%), m.p. 130.0–131.0 °C. ¹H NMR (DMSO-*d*₆, 300 MHz): 6.83 (d, *J* = 7.9 Hz, 1H), 6.80 (s, 1H), 6.71 (d, *J* = 7.8 Hz, 1H), 6.17 (t, *J* = 5.8 Hz, 1H), 5.96 (s, 2H), 5.84 (t, *J* = 5.5 Hz, 1H), 4.09 (d, *J* = 6.0 Hz, 2H), 2.99 (q, *J* = 6.7 Hz, 2H), 1.36 – 1.25 (m, 8H), 0.86 (t, *J* = 6.5 Hz, 3H). ¹³C NMR (DMSO-*d*₆, 75 MHz): 158.2, 147.9, 146.8, 133.3, 120.6, 108.2, 108.1, 101.0, 44.4, 40.6, 31.5, 30.1, 26.5, 22.5, 14.0. HPLC analyses: 96.7%.

1-(benzo[d][1,3]dioxol-5-ylmethyl)-3-phenylthiourea (6a):

White solid (Yield: 40%), m.p. 160.3–162.1 °C. ¹H NMR (CDCl₃, 300 MHz): 7.72 (s, 1H), 7.41 (t, *J* = 7.7 Hz, 2H), 7.28 – 7.21 (m, 1H), 7.19 (d, *J* = 7.6 Hz, 2H), 6.81 (s, 1H), 6.74 (s, 2H), 6.17 (bs, 1H), 5.94 (s, 2H), 4.77 (d, *J* = 5.4 Hz, 2H). ¹³C NMR (CDCl₃, 75 MHz): 180.2, 147.2, 146.3, 141.9, 131.9, 124.4, 121.0, 120.6, 108.3, 108.1, 100.9, 54.8, 47.0. HPLC analyses: 99.9%.

1-(benzo[d][1,3]dioxol-5-ylmethyl)-3-(4-nitrophenyl)thiourea (6b):

Yellow solid (Yield: 50%), m.p. 142.1–143.9 °C. ¹H NMR (DMSO-*d*₆, 300 MHz): 10.16 (s, 1H), 8.58 (bs, 1H), 8.19 (d, *J* = 9.2 Hz, 2H), 7.86 (d, *J* = 9.2 Hz, 2H), 6.96 (s, 1H), 6.90 (d, *J* = 7.9 Hz, 1H), 6.86 (d, *J* = 8.0 Hz, 1H), 6.00 (s, 2H), 4.66 (d, *J* = 4.0 Hz, 2H). ¹³C NMR (DMSO-*d*₆, 75 MHz): 180.7, 147.2, 146.2, 138.3, 132.6, 128.4, 128.0, 124.8, 120.8, 108.1, 108.0, 100.8, 46.9. HPLC analyses: 99.5%.

1-(benzo[d][1,3]dioxol-5-ylmethyl)-3-(4-chlorophenyl)thiourea (6c):

White solid (Yield: 65%), m.p. 151.0–152.5 °C. ¹H NMR (CDCl₃, 300 MHz): 7.73 (s, 1H), 7.37 (d, *J* = 8.6 Hz, 2H), 7.14 (d, *J* = 8.6 Hz, 2H), 6.81 (s, 1H), 6.74 (s, 2H), 6.09 (bs, 1H), 5.94 (s, 2H), 4.74 (d, *J* = 5.4 Hz, 2H). ¹³C NMR (DMSO-*d*₆, 75 MHz): 180.6, 147.1, 146.1, 139.1, 132.7, 128.6, 124.4, 123.4, 120.8, 108.1, 108.0, 100.8, 46.9. HPLC analyses: 99.8%.

1-(benzo[d][1,3]dioxol-5-ylmethyl)-3-(4-methoxyphenyl)thiourea (6d):

White solid (Yield: 90%), m.p. 161.1–162.5 °C. ¹H NMR (DMSO-*d*₆, 300 MHz): 9.33 (s, 1H), 7.82 (s, 1H), 7.27 (d, *J* = 8.4 Hz, 2H), 6.92 (d, *J* = 4.2 Hz, 2H), 6.88 (d, *J* = 7.3 Hz, 2H), 6.85 (d, *J* = 5.9 Hz, 1H), 6.79 (s, 1H), 5.97 (s, 2H), 4.64 (d, *J* = 4.5 Hz, 2H), 3.74 (s, 3H). ¹³C NMR (DMSO-*d*₆, 75 MHz): 183.3, 158.8, 148.6, 147.6, 134.1, 127.9, 121.8, 115.3, 109.1, 108.7, 101.9, 55.7, 48.7. HPLC analyses: 99.0%.

1-(benzo[d][1,3]dioxol-5-ylmethyl)-3-(p-tolyl)thiourea (6e):

White solid (Yield: 48%), m.p. 135.0–137.0 °C. ¹H NMR (DMSO-*d*₆, 300 MHz): 9.45 (s, 1H), 7.95 (bs, 1H), 7.23 (d, *J* = 8.3 Hz, 2H), 7.13 (d, *J* = 8.3 Hz, 2H), 6.93 (s, 1H), 6.87 (d, *J* = 7.9 Hz, 1H), 6.82 (d, *J* = 8.0 Hz, 1H), 5.99 (s, 2H), 4.62 (d, *J* = 5.7 Hz, 2H), 2.28 (s, 3H). ¹³C NMR (DMSO-*d*₆, 75 MHz): 180.7, 147.1, 146.1,

136.4, 133.7, 132.9, 129.1, 123.0, 120.7, 108.1, 107.9, 100.8, 46.9, 20.4. HPLC analyses: 96.4%.

1-(benzo[d][1,3]dioxol-5-ylmethyl)-3-butylthiourea (6f):

Yellow solid (Yield: 75%), m.p. 71.2–73.0 °C. ¹H NMR (DMSO-*d*₆, 300 MHz): 7.68 (bs, 1H), 7.41 (bs, 1H), 6.85 (d, *J* = 10.1 Hz, 2H), 6.76 (d, *J* = 7.9 Hz, 1H), 5.97 (s, 2H), 4.54 (d, *J* = 6.0 Hz, 2H), 1.50 – 1.40 (m, 2H), 1.34 – 1.21 (m, 4H), 0.87 (t, *J* = 7.3 Hz, 3H). ¹³C NMR (DMSO-*d*₆, 75 MHz): 177.4, 147.1, 146.0, 133.2, 120.5, 107.9, 100.7, 46.6, 43.2, 30.8, 19.5, 13.6. HPLC analyses: 99.1%.

1-(benzo[d][1,3]dioxol-5-ylmethyl)-3-hexylthiourea (6g):

White solid (Yield: 52%), m.p. 116.0–117.0 °C. ¹H NMR (DMSO-*d*₆, 300 MHz): 7.69 (bs, 1H), 7.42 (bs, 1H), 6.87 (s, 1H), 6.85 (d, *J* = 9.0 Hz, 1H), 6.76 (d, *J* = 9.3 Hz, 1H), 5.98 (s, 2H), 4.54 (d, *J* = 4.2 Hz, 2H), 1.45 (q, *J* = 6.6 Hz, 2H), 1.33 – 1.25 (m, 8H), 0.87 (t, *J* = 6.7 Hz, 3H). ¹³C NMR (DMSO-*d*₆, 75 MHz): 158.2, 147.9, 146.8, 133.3, 120.6, 108.2, 108.1, 101.0, 44.4, 40.6, 31.5, 30.1, 26.5, 22.5, 14.0. HPLC analyses: 99.8%.

1-(4-hydroxy-3-methoxybenzyl)-3-phenylurea (7a):

White solid (Yield: 42%), m.p. 181.7–183.2 °C. ¹H NMR (DMSO-*d*₆, 300 MHz): 8.79 (s, 1H), 8.47 (s, 1H), 7.40 (d, *J* = 7.9 Hz, 2H), 7.21 (t, *J* = 7.8 Hz, 2H), 6.90 (t, *J* = 8.1 Hz, 2H), 6.75 (s, 1H), 6.72 (s, 1H), 6.46 (t, *J* = 4.8 Hz, 1H), 4.19 (d, *J* = 5.1 Hz, 2H), 3.75 (s, 3H). ¹³C NMR (DMSO-*d*₆, 75 MHz): 155.1, 147.5, 145.5, 140.5, 130.9, 128.6, 121.0, 119.7, 117.6, 115.3, 111.8, 55.6, 42.7. HPLC analyses: 99.6%.

1-(4-hydroxy-3-methoxybenzyl)-3-(4-nitrophenyl)urea (7b):

Yellow solid (Yield: 48%), m.p. 187.0–183.2 °C. ¹H NMR (DMSO-*d*₆, 300 MHz): 8.79 (bs, 1H), 8.32 (s, 1H), 7.27 (d, *J* = 8.1 Hz, 2H), 7.02 (d, *J* = 8.1 Hz, 2H), 6.87 (s, 1H), 6.75 – 6.68 (m, 2H), 6.38 (t, *J* = 5.4 Hz, 1H), 4.17 (d, *J* = 5.4 Hz, 2H), 3.75 (s, 3H). ¹³C NMR (DMSO-*d*₆, 75 MHz): 155.2, 147.5, 145.4, 137.9, 131.0, 129.7, 129.0, 119.7, 117.8, 115.3, 111.8, 55.6, 42.7. HPLC analyses: 95.0%.

1-(4-chlorophenyl)-3-(4-hydroxy-3-methoxybenzyl)urea (7c):

White solid (Yield: 59%), m.p. 198.4–199.9 °C. ¹H NMR (DMSO-*d*₆, 300 MHz): 8.80 (bs, 1H), 8.61 (s, 1H), 7.44 (d, *J* = 7.4 Hz, 2H), 7.25 (d, *J* = 7.4 Hz, 2H), 6.87 (s, 1H), 6.73 (d, *J* = 9.0 Hz, 1H), 6.70 (d, *J* = 9.0 Hz, 1H), 6.50 (t, *J* = 5.0 Hz, 1H), 4.18 (d, *J* = 4.8 Hz, 2H), 3.75 (s, 3H). ¹³C NMR (DMSO-*d*₆, 75 MHz): 154.9, 147.5, 145.5, 139.5, 130.8, 128.4, 124.5, 119.8, 119.1, 115.3, 113.6, 55.7, 42.7. HPLC analyses: 99.8%.

1-(4-hydroxy-3-methoxybenzyl)-3-(4-methoxyphenyl)urea (7d):

White solid (Yield: 72%), m.p. 154.9–156.8 °C. ¹H NMR (DMSO-*d*₆, 300 MHz): 8.81 (s, 1H), 8.25 (s, 1H), 7.31 (d, *J* = 8.9 Hz, 2H), 6.88 (s, 1H), 6.82 (d, *J* = 8.9 Hz, 2H), 6.74 (d, *J* = 8.2 Hz, 1H), 6.71 (d, *J* = 9.0 Hz, 1H), 6.34 (t, *J* = 5.6 Hz, 1H), 4.18 (d, *J* = 5.7 Hz, 2H), 3.76 (s, 3H), 3.70 (s, 3H). ¹³C NMR (DMSO-*d*₆, 75 MHz):

155.4, 154.0, 147.4, 145.4, 133.6, 131.1, 119.7, 119.5, 115.3, 113.9, 111.8, 55.6, 55.1, 42.7. HPLC analyses: 99.4%.

1-(4-hydroxy-3-methoxybenzyl)-3-(p-tolyl)urea (7e):

White solid (Yield: 63%), m.p. 198.4–199.5 °C. ¹H NMR (DMSO-*d*₆, 300 MHz): 8.80 (bs, 1H), 8.32 (s, 1H), 7.27 (d, *J* = 7.6 Hz, 2H), 7.02 (d, *J* = 8.0 Hz, 2H), 6.87 (s, 1H), 6.73 (d, *J* = 8.0 Hz, 1H), 6.69 (d, *J* = 9.0 Hz, 1H), 6.38 (t, *J* = 5.1 Hz, 1H), 4.17 (d, *J* = 5.2 Hz, 2H), 3.17 (s, 3H), 2.12 (s, 3H). ¹³C NMR (DMSO-*d*₆, 75 MHz): 154.9, 147.5, 145.5, 139.5, 130.8, 128.4, 124.5, 119.8, 119.1, 115.3, 113.6, 55.7, 42.7. HPLC analyses: 98.6%.

1-butyl-3-(4-hydroxy-3-methoxybenzyl)urea (7f):

White solid (Yield: 20%), m.p. 96.7–98.5 °C. ¹H NMR (DMSO-*d*₆, 300 MHz): 8.76 (bs, 1H), 6.81 (s, 1H), 7.60 (d, *J* = 7.9 Hz, 1H), 6.63 (d, *J* = 7.8 Hz, 1H), 6.11 (bs, 1H), 5.84 (bs, 1H), 4.08 (s, 2H), 3.73 (s, 3H), 1.39 – 1.16 (m, 6H), 0.86 (t, *J* = 7.1 Hz, 3H). ¹³C NMR (DMSO-*d*₆, 75 MHz): 158.1, 147.4, 145.2, 131.7, 119.5, 115.2, 111.6, 55.8, 55.5, 42.8, 32.2, 19.5, 13.7. HPLC analyses: 98.3%.

1-hexyl-3-(4-hydroxy-3-methoxybenzyl)urea (7g):

Yellow solid (Yield: 42%), m.p. 83.4–84.3 °C. ¹H NMR (DMSO-*d*₆, 300 MHz): 6.79 (d, *J* = 8.0 Hz, 1H), 6.79 (s, 1H), 6.68 (d, *J* = 8.0 Hz, 1H), 6.02 (s, 1H), 5.26 (t, *J* = 5.3 Hz, 1H), 4.98 (t, *J* = 5.0 Hz, 1H), 4.17 (d, *J* = 5.5 Hz, 2H), 3.79 (s, 3H), 3.08 (q, *J* = 6.7 Hz, 2H), 1.43 – 1.36 (m, 8H), 0.89 (t, 3H). ¹³C NMR (DMSO-*d*₆, 75 MHz): 158.8, 146.8, 144.9, 131.2, 120.2, 114.4, 110.3, 55.8, 44.3, 40.5, 31.5, 30.2, 26.5, 22.5, 14.0. HPLC analyses: 98.8%.

1-(4-hydroxy-3-methoxybenzyl)-3-phenylthiourea (8a):

White solid (Yield: 37%), m.p. 131.4–133.3 °C. ¹H NMR (DMSO-*d*₆, 300 MHz): 9.50 (s, 1H), 8.84 (s, 1H), 7.98 (s, 1H), 7.46 (d, *J* = 7.4 Hz, 2H), 7.34 (d, *J* = 7.3 Hz, 2H), 7.12 (t, *J* = 7.1 Hz, 1H), 6.96 (s, 1H), 6.76 (d, *J* = 6.7 Hz, 2H), 4.61 (d, *J* = 4.6 Hz, 2H), 3.76 (s, 3H). ¹³C NMR (DMSO-*d*₆, 75 MHz): 180.5, 147.5, 145.7, 139.3, 129.5, 128.5, 124.1, 123.2, 120.3, 115.3, 112.3, 55.6, 47.3. HPLC analyses: 99.8%.

1-(4-hydroxy-3-methoxybenzyl)-3-(4-nitrophenyl)thiourea (8b):

Yellow solid (Yield: 39%), m.p. 163.7–164.9 °C. ¹H NMR (DMSO-*d*₆, 300 MHz): 10.13 (s, 1H), 8.90 (bs, 1H), 8.50 (s, 1H), 8.17 (d, *J* = 9.2 Hz, 2H), 7.87 (d, *J* = 9.2 Hz, 2H), 6.97 (s, 1H), 6.79 (d, *J* = 8.2 Hz, 2H), 6.75 (d, *J* = 8.0 Hz, 1H), 4.61 (d, *J* = 5.1 Hz, 2H), 3.77 (s, 3H). ¹³C NMR (DMSO-*d*₆, 75 MHz): 179.9, 147.5, 146.4, 145.9, 141.8, 128.6, 124.4, 120.5, 115.3, 112.4, 55.7, 47.3. HPLC analyses: 99.1%.

1-(4-chlorophenyl)-3-(4-hydroxy-3-methoxybenzyl)thiourea (8c):

White solid (Yield: 51%), m.p. 154.0–154.7 °C. ¹H NMR (DMSO-*d*₆, 300 MHz): 9.56 (s, 1H), 8.85 (bs, 1H), 8.08 (s, 1H), 7.50 (d, *J* = 8.6 Hz, 2H), 7.35 (d, *J* = 8.6 Hz, 2H), 6.95 (s, 1H), 6.77 (d, *J* = 9.3 Hz, 1H), 6.74 (d, *J* = 8.2 Hz, 1H), 4.60 (d, *J* = 5.1 Hz, 2H), 3.76 (s, 3H). ¹³C NMR (DMSO-*d*₆, 75 MHz): 180.5, 147.5, 145.7, 138.4, 129.3, 128.3, 127.8, 124.6, 120.3, 115.3, 112.3, 55.6, 47.3. HPLC analyses: 98.5%.

1-(4-hydroxy-3-methoxybenzyl)-3-(4-methoxyphenyl)thiourea (8d):

White solid (Yield: 56%), m.p. 140.0–141.3 °C. ¹H NMR (DMSO-*d*₆, 300 MHz): 9.30 (s, 1H), 8.82 (s, 1H), 7.77 (bs, 1H), 7.25 (d, *J* = 8.8 Hz, 2H), 6.93 (s, 1H), 6.89 (d, *J* = 8.8 Hz, 2H), 4.58 (d, *J* = 5.1 Hz, 2H), 3.75 (s, 3H), 3.73 (s, 3H). ¹³C NMR (DMSO-*d*₆, 75 MHz): 180.9, 156.5, 147.4, 145.6, 131.8, 129.7, 125.9, 120.1, 115.2, 113.9, 112.1, 55.6, 55.2, 47.2. HPLC analyses: 98.8%.

1-(4-hydroxy-3-methoxybenzyl)-3-(p-tolyl)thiourea (8e):

White solid (Yield: 48%), m.p. 131.4–133.3 °C. ¹H NMR (DMSO-*d*₆, 300 MHz): 7.89 (s, 1H), 7.18 (d, *J* = 8.0 Hz, 2H), 7.07 (d, *J* = 8.2 Hz, 2H), 6.87 (s, 1H), 6.83 (d, *J* = 8.0 Hz, 1H), 6.74 (d, *J* = 8.0 Hz, 1H), 6.14 (bs, 1H), 5.63 (s, 1H), 4.76 (d, *J* = 5.3 Hz, 2H), 3.86 (s, 3H), 2.33 (s, 3H). ¹³C NMR (DMSO-*d*₆, 75 MHz): 180.8, 146.7, 145.3, 137.6, 133.2, 130.8, 129.2, 125.5, 120.8, 114.5, 110.7, 56.0, 49.4, 21.0. HPLC analyses: 99.3%.

1-hexyl-3-(4-hydroxy-3-methoxybenzyl)thiourea (8f):

White solid (Yield: 22%), m.p. 81.1–82.0 °C. ¹H NMR (CDCl₃, 300 MHz): 6.89 – 6.87 (m, 2H), 6.80 (d, *J* = 8.0 Hz, 1H), 6.01 (bs, 1H), 5.80 (bs, 1H), 5.65 (s, 1H), 4.55 (s, 2H), 3.88 (s, 3H), 3.35 (d, *J* = 4.1 Hz, 2H), 1.60 – 1.48 (m, 8H), 0.86 (d, *J* = 6.1 Hz, 3H). ¹³C NMR (CDCl₃, 75 MHz): 181.7, 147.0, 145.6, 128.7, 120.7, 114.6, 110.4, 56.0, 48.6, 44.4, 31.4, 28.8, 26.5, 22.5, 13.9. HPLC analyses: 97.3%.

Biological Assays**Cytotoxic activity**

All compounds were submitted to cytotoxic activity assays in tumorigenic and non-tumorigenic cell lines. The tumorigenic cell lines were murine melanoma (B16F10), human melanoma (SK-MEL-25 and A2058), human glioblastoma (U-87), human mammary adenocarcinoma (MCF-7), human cervical adenocarcinoma (HeLa), and human fibroblast (T75) as non-tumorigenic cell line. The MTT assay was used to evaluate cell viability and proliferation. Cells in the logarithmic growth phase were plated at a density of 10⁴ cells/mL in 96-well plates. 24 hours later, cells were treated with capsaicin and compounds **5a-5g**, **6a-6g**, **7a-7g** and **8a-8f** at the concentrations of 3.0 to 100 μM for further 24 h. Then, 5 μL of MTT (5 mg/mL) was then added to each well and incubated again under same conditions for 3 h. Subsequently, 100 μL of 30% sodium dodecyl sulfate (SDS) was added and plates were stored overnight. Then, the absorbance was quantified at 570 nm by spectrophotometry (Spectramax-M2, Software Molecular Pro 5.4, Sunnyvale, CA, EUA).⁶⁹ Cell viability was expressed as percentage values compared to the negative control.

$$\% \text{ viable cells} = \frac{(Aa - Ab) \times 100}{Ac - Ab}$$

Aa: sample absorbance; Ab: negative control absorbance; Ac: positive control absorbance.

The data were plotted on Prism 5 software version 5.03 (GraphPad Software, Inc, 2009), where the IC₅₀ was calculated according to the tutorial provided by Prism.

Cell cycle analysis

B16F10 murine melanoma and A2058 human melanoma cells were plated in 12-well plates at the concentration of 10⁵ cells/well. For synchronization, the cells were plated with RPMI medium without addition of fetal bovine serum (FBS). After 12 h of incubation, the FBS-free medium was removed and the cells were treated with the highest activity analog **6g** at concentrations relative to the IC₅₀ value, diluted in RPMI medium supplemented with 10% FBS and incubated in an oven containing 5% CO₂ at 37 °C. After 24 h of incubation, cells were washed with PBS and centrifuged for 10 min at 1200 RPM. The pellet was resuspended in 300 µL of HSF (0.1% Triton X-100, 0.1% sodium citrate of 50 µg/mL propidium iodide), 10 µg/mL RNase (Sigma-Aldrich) and incubated at 37 °C for 1 h in the absence of light. Data were acquired by flow cytometry (FACSCalibur). The Dean Jett-Fox algorithm of the FlowJo software (TreeStar Inc, Ashland, OR, USA) was used to determine the percentage of cells in the home phase of the cycle.

Analysis of cell signaling induced by the compound **6g**

For analysis of cell cycle and cell migration mediators, Western blotting assay was standardized from the cell lysates obtained from the culture of A2058 melanoma cells treated with the **6g**. Proteins from each sample were separated by gel (10% SDS-PAGE) electrophoresis using buffer 2.5 mM Tris-HCl (pH 8.0), 19 mM glycine and 0.3 mM SDS. The samples were then transferred to nitrocellulose membranes (Protran, Schleicher and Schuell, USA) in buffer containing 1.2 mM Tris-HCl (pH 8.0), 9.6 mM glycine and 20% methanol.

The efficacy of the blots was verified by staining the membranes with Ponceau S (Sigma) dye, followed by blocking in solution containing 5% milk powder (Nestlé, Brazil) diluted in PBS. After the blockade, (3x) 10 min washes were performed with TTBS (20 mM Tris-HCl (pH 7.6), 150 mM NaCl and 0.1% Tween 20 (pH 7.6) for 2 h. After washing, membranes were incubated for 24 h at 4 °C under constant stirring and with the following primary antibodies: Anti-Cyclin D1 mouse, anti-Cyclin D3 mouse, anti-Cyclin A mouse, antiNFκ-B rabbit, anti-fosfo Akt (Thr308) rabbit, anti-β-Catenin rabbit, anti-c-Raf, antifosfo c-Ras, anti-fosfo p38 (Thr180/Tyr182) rabbit, anti-fosfo MAPK rabbit, anti-fosfo GSK3β (Ser9) rabbit; anti-N-Cadherin rabbit, anti-Src rabbit, anti-fosfo Src (Tyr416) rabbit, anti-FAK rabbit, anti-fosfo FAK (Tyr925) rabbit and anti-fosfo FAK (Tyr397) rabbit. All primary antibodies were purchased from Cell Signaling Technology (Beverly, MA). After incubation with the primary antibodies, membranes were washed with TTBS for 30 min and incubated for 1 h at room temperature under stirring with the secondary antibody conjugated with IgG horseradish peroxidase, purchased from Sigma-Aldrich (St. Louis, MO). Then, membranes were washed with TTBS and the Luminata™ chemiluminescent substrate was added and the membranes were developed and analyzed in ImageQuant LAS4000 (GE) Photodocumentator system. All bands were normalized in comparison with β-actin.

FLIPR assays – TRPV1/6 activity

Cell culture reagents and Lipofectamine 2000 were purchased from Invitrogen Life Technologies Europe B.V. The calcium indicator, Calcium-5 was bought from Molecular Devices LLC. All other chemicals were purchased from Sigma-Aldrich.

HEK293T cells (ATCC) were cultured at 37 °C in DMEM cell culture media supplemented with 10% FBS, 10 mM HEPES, 1 mM sodium pyruvate, and 1% penicillin/streptomycin. The attached cells were trypsinized and plated at 27,000 cells/well density onto Corning® 96-well black polystyrene clear bottom microplates (CLS3603 Sigma-Aldrich) coated with 100 µg/mL poly-D-lysine (P6407 Sigma-Aldrich) using 100 µL phenol-red free DMEM with 10% FBS and 2 mM glutamine without antibiotics. Transfection was performed 24 h later using 200 ng of TRPV1-pcDNA 3.1 and 0.6 µL Lipofectamine 2000 reagent/well.

TRPV1 activity was measured using HEK293T cells transiently overexpressing TRPV1 as previously reported.⁵⁷ 24 h after the transfection, the medium was replaced

with 90 μL of loading buffer (modified Krebs buffer containing 117 mM NaCl, 4.8 mM KCl, 1 mM MgCl_2 , 5 mM D-glucose, 10 mM HEPES, 1.8 mM CaCl_2 and calcium-5 fluorescence dye (50 $\mu\text{L}/\text{mL}$ loading buffer). Cells were incubated in the loading buffer at 37 $^\circ\text{C}$ for 1 h in dark. Fluorescence Ca^{2+} measurements were carried out using FLIPR^{TETRA} high-throughput, fluorescence microplate reader. Cells were excited using a 470–495 nm LED module, and the emitted fluorescence signal was filtered with a 515–575 nm emission filter (manufacturer's guidelines). Stable baselines were established for 50 seconds before 10 μL of a 10X compound prepared in 1.8 mM CaCl_2 -containing Krebs buffer was robotically administered to the cells. Cells were incubated and fluorescence was monitored in the presence of compound for an additional 5 minutes before administration of 100 μL of 2X capsaicin or **6g** prepared in 1.8 mM CaCl_2 -containing Krebs buffer (final concentration of capsaicin in the assay plate was 100 nM). The activity of TRPV1 was measured by quantifying the area under the curve (AUC) of the fluorescence intensity, following administration of the agonists.

HEK293 cells stably over-expressing *hTRPV6* (HEK-TRPV6, previously established⁵⁸) were seeded at a density of 70,000 cells per well onto Corning[®] 96-well black polystyrene clear bottom microplates coated with 100 $\mu\text{g}/\text{mL}$ poly-D-lysine using 100 μL phenol-red free DMEM with 10% FBS and 2 mM glutamine without antibiotics.

TRPV6 activity was measured using the HEK-TRPV6 cell line as previously reported.^{59,70} 16 h later the medium was replaced with 50 μL of nominally calcium-free (NCF) loading buffer (modified Krebs buffer containing 117 mM NaCl, 4.8 mM KCl, 1 mM MgCl_2 , 5 mM D-glucose, 10 mM HEPES, and calcium-5 fluorescence dye (50 μL per mL loading buffer). Cells were incubated in the NCF-loading buffer at 37 $^\circ\text{C}$ for 1 h in dark. Fluorescence Cd^{2+} measurements were carried out using FLIPR^{TETRA} high-throughput, fluorescence microplate reader. Cells were excited using a 470–495 nm LED module, and the emitted fluorescence signal was filtered with a 515–575 nm emission filter (manufacturer's guidelines). Stable calcium-free baselines were established for 50 seconds before 50 μL of 3X compound either *cis*-22a or **6g** was robotically administered to the cells. Cells were incubated and fluorescence was monitored in the presence of compound for an additional 5 minutes before administration of 50 μL of a 4X CdCl_2 substrate (final concentration of CdCl_2 in the assay plate was 50 μM). The activity of *hTRPV6* was measured by quantifying the AUC of the fluorescence intensity following administration of the substrate.

Experiments were done with 3 to 6 repeats per group on at least two different days. Relative IC₅₀ values were determined using GraphPad® Prism (GraphPad® Software, v. 5.0, San Diego, CA, US). Inhibition curves were obtained by non-linear regression using the built-in log (inhibitor) *versus* normalized response function.

Assessment of the nociceptive behavior induced by compound 6g

Male Swiss mice, weighting between 18 to 20 g, were housed in a room with controlled temperature (22 ± 2 °C) and lighting (lights on from 6 am to 6 pm), with free access to water and food. All experiments were conducted between 9 am and 5 pm and were in accordance with the ethical guidelines of the International Association for the Study of Pain.⁷¹ Mice were individually positioned in a fully transparent box with an upper opening for air intake. Animal remained for 20 min for its adaptation prior to the experiment. Capsaicin, compound **6g** (5.2 nmol/paw, 20 µL) and the corresponding vehicle (EtOH + saline), under the same experimental conditions, were administered by the intraplantar route. Immediately after injection, the animal returned to the transparent box positioned in front of a mirror to facilitate viewing and measuring the time (in seconds) of flinches or licks of the treated paw for 5 min.⁵³ The animal assays were approved by the Ethics Committee for the use of animals of the Butantan Institute, under the protocol number: 1904030518.

Statistical analysis

Statistical analysis was performed using analysis of variance⁷² associated with the Tukey test⁷³ for comparison of more than two means. The significance level was $p < 0.05$.

Molecular modeling approach

The three-dimensional (3D) molecular models of capsaicin and its derivative were built up, in their neutral forms, using ChemBio Draw® Ultra 12.0 and the electronic, steric, topological and lipophilicity properties were calculated by Spartan'14®

software. Energy minimization was performed by semi-empirical method PM6, followed by Hartree-Fock 3-21G method, thus obtaining the descriptors: electrostatic potential maps (EPM), energy of the frontier orbitals HOMO and LUMO, calculated partition coefficient (ClogP), hydrogen bond acceptor (HBA), hydrogen bond donor (HBD), polar surface area (PSA), and dipole moment (μ).

Reverse virtual screening approach

In order to find possible targets for the most promising compound **6g**, a virtual screening strategy was employed. Compound **6g** was simplified (**6g_mod**) by removing its aliphatic chain attached to the thiourea linker and then compared to all ligands bound to proteins available on PDB. This task was accomplished using the software PharmACOPhore⁷⁴ and ShaEP.⁷⁵ The first software changed **6g_mod** conformation to align it to all the co-crystallographic ligands available on PDB. The latter was used to quantitatively express the shape and electrostatic similarity between aligned **6g_mod** and the PDB ligands. **6g** was simplified to reduce biasing the alignment to the aliphatic portion. This approach helped to find possible targets for **6g**, since similar compounds tend to have similar biological activities. The top best cancer-related targets were filtered out and analyzed *via* molecular docking with AutoDock Vina.⁷⁶

Conflict of Interest

The authors declare no conflict of interest.

Acknowledgements

The authors are grateful to Faculty of Pharmacy of University of São Paulo, which allowed the development of this work and to Coordenação de Aperfeiçoamento de Pessoal de Nível Superior (CAPES), Conselho Nacional de Desenvolvimento Científico e Tecnológico (CNPq) and Fundação de Amparo à Pesquisa do Estado de São Paulo (FAPESP, grant numbers: 2013/19311-6 and 2017/00689-0) for financial support. R.B. and M.A.H. acknowledge the SNF Sinergia grant number: CRSII5_180326 for the funding to support this work. M.R.C. acknowledge the Swiss Excellence Scholarship for Foreign Students and Scholars (ESKAS – 2017.0670). The authors are also grateful to Guilherme Galdino for technical assistance in biological

assays. The human TRPV1 plasmid was a kind gift from Dr. Yoshiro Suzuki, Department of Physiology, Iwate Medical University, Japan and Dr. Makoto Tominaga, Division of Cellular Signaling, Okazaki Institute for Integrative Bioscience, Japan.

Supplementary material

¹H and ¹³C NMR spectra, HPLC, and supplementary figures are available online at <https://doi.org/10.1016/>

References

1. Hanahan D, Weinberg RA. Hallmarks of cancer: The next generation. *Cell*. 2011;144(5):646-674. doi:10.1016/j.cell.2011.02.013.
2. World Health Organization: Cancer. <<http://www.who.int/mediacentre/factsheets/fs297/en/>> Accessed Jan 16, 2019.
3. Murthy YLN, Suhasini KP, Pathania AS, Bhushan S, Nagendra Sastry Y. Synthesis, structure activity relationship and mode of action of 3-substitutedphenyl-1-(2,2,8,8-tetramethyl-3,4,9,10-tetrahydro-2H,8H-pyrano[2, 3-f]chromen-6-yl)-propenones as novel anticancer agents in human leukaemia HL-60 cells. *Eur J Med Chem*. 2013;62:545-555. doi:10.1016/j.ejmech.2013.01.027.
4. Castro-Castillo V, Suárez-Rozas C, Castro-Loiza N, Theoduloz C, Cassels BK. Annulation of substituted anthracene-9,10-diones yields promising selectively antiproliferative compounds. *Eur J Med Chem*. 2013;62:688-692. doi:10.1016/j.ejmech.2013.01.049.
5. Newman DJ, Cragg GM. Natural Products as Sources of New Drugs from 1981 to 2014. *J Nat Prod*. 2016;79(3):629-661. doi:10.1021/acs.jnatprod.5b01055.
6. Surh Y. More Than Spice : Capsaicin in Hot Chili Peppers Makes Tumor Cells Commit Suicide. *J Natl Cancer Inst*. 2002;94(17):1263-1265. doi:10.1093/jnci/94.17.1263.
7. Min JK, Han KY, Kim EC, et al. Capsaicin Inhibits in Vitro and in Vivo Angiogenesis. *Cancer Res*. 2004;64(2):644-651. doi:10.1158/0008-5472.CAN-03-3250.
8. Luo XJ, Peng J, Li YJ. Recent advances in the study on capsaicinoids and capsinoids. *Eur J Pharmacol*. 2011;650(1):1-7. doi:10.1016/j.ejphar.2010.09.074.
9. Díaz-Laviada I, Rodríguez-Henche N. The potential antitumor effects of capsaicin. *Prog Drug Res*. 2014;68:181-208.
10. José Díaz FP, Merino AB& F. Peroxidases and the metabolism of capsaicin in *Capsicum annuum* L. José. *Phytochem Rev*. 2009;3(August):2008-2009.

11. Simone DA, Baumann TK, LaMotte RH. Dose-dependent pain and mechanical hyperalgesia in humans after intradermal injection of capsaicin. *Pain*. 1989;38(1):99-107. doi:10.1016/0304-3959(89)90079-1.
12. Brederson JD, Kym PR, Szallasi A. Targeting TRP channels for pain relief. *Eur J Pharmacol*. 2013;716(1-3):61-76. doi:10.1016/j.ejphar.2013.03.003.
13. Galano A, Mart??nez A. Capsaicin, a tasty free radical scavenger: Mechanism of action and kinetics. *J Phys Chem B*. 2012;116(3):1200-1208. doi:10.1021/jp211172f.
14. Jun HS, Park T, Lee CK, et al. Capsaicin induced apoptosis of B16-F10 melanoma cells through down-regulation of Bcl-2. *Food Chem Toxicol*. 2007;45(5):708-715. doi:10.1016/j.fct.2006.10.011.
15. Friedman JR, Nolan NA, Miles SL, et al. Anti-cancer Activity of Natural and Synthetic Capsaicin Analogs. *J Pharmacol Exp Ther*. 2017;386(1). doi:10.1124/jpet.117.243691.
16. Walpole CSJ, Wrigglesworth R, Bevan S, et al. Analogs of capsaicin with agonist activity as novel analgesic agents; structure-activity studies. 1. The aromatic "A-region"; *J Med Chem*. 1993;36(16):2362-2372. doi:10.1021/jm00068a014.
17. Walpole CSJ, Wrigglesworth R, Bevan S, et al. Analogs of capsaicin with agonist activity as novel analgesic agents; structure-activity studies. 2. The amide bond "B-region"; *J Med Chem*. 1993;36(16):2373-2380. doi:10.1021/jm00068a015.
18. Walpole CSJ, Wrigglesworth R, Bevan S, et al. Analogs of capsaicin with agonist activity as novel analgesic agents; structure-activity studies. 3. The hydrophobic side-chain "C-region"; *J Med Chem*. 1993;36(16):2381-2389. doi:10.1021/jm00068a016.
19. Janusz JM, Buckwalter BL, Young PA, et al. Vanilloids. 1. Analogs of capsaicin with antinociceptive and antiinflammatory activity. *J Med Chem*. 1993;36(18):2595-2604. doi:10.1021/jm00070a002.
20. Appendino G, Mu??oz E, Fiebich BL. TRPV1 (vanilloid receptor, capsaicin receptor) agonists and antagonists. *Expert Opin Ther Pat*. 2003;13(12):1825-1837. doi:10.1517/13543776.13.12.1825.
21. Gharat LA, Szallasi A. Advances in the design and therapeutic use of capsaicin receptor TRPV1 agonists and antagonists. *Expert Opin Ther Pat*. 2008;18(2):159-209. doi:10.1517/13543776.18.2.159.
22. Huang X-F, Xue J-Y, Jiang A-Q, Zhu H-L. Capsaicin and Its Analogues: Structure-Activity Relationship Study. *Curr Med Chem*. 2013;20(21):2661-2672. doi:10.2174/0929867311320210004.
23. Clark R, Lee S. Anticancer Properties of Capsaicin Against Human Cancer. *Anticancer Res*. 2016;36(3):837-843.
24. Huang S-P, Chen J-C, Wu C-C, et al. Capsaicin-induced apoptosis in human hepatoma HepG2 cells. *Anticancer Res*. 2009;29(1):165-174.

25. Xie L, Xiang GH, Tang T, et al. Capsaicin and dihydrocapsaicin induce apoptosis in human glioma cells via ROS and Ca²⁺-mediated mitochondrial pathway. *Mol Med Rep*. 2016;14(5):4198-4208. doi:10.3892/mmr.2016.5784.
26. Lin C-H, Lu W-C, Wang C-W, Chan Y-C, Chen M-K. Capsaicin induces cell cycle arrest and apoptosis in human KB cancer cells. *BMC Complement Altern Med*. 2013;13(1):46. doi:10.1186/1472-6882-13-46.
27. Ziglioli F, Frattini A, Maestroni U, Dinale F, Ciuffreda M, Cortellini P. Vanilloid-mediated apoptosis in prostate cancer cells through a TRPV-1 dependent and a TRPV-1-independent mechanism. *Acta Biomed l'Ateneo Parm*. 2009;80(1):13-20.
28. De-Sá-Júnior PL, Pasqualoto KFM, Ferreira AK, et al. RPF101, A new capsaicin-like analogue, Disrupts the microtubule network accompanied by arrest in the G2/M phase, Inducing apoptosis and mitotic catastrophe in the MCF-7 breast cancer cells. *Toxicol Appl Pharmacol*. 2013;266(3):385-398. doi:10.1016/j.taap.2012.11.029.
29. Ferreira AK, Tavares MT, Pasqualoto KFM, et al. RPF151, a novel capsaicin-like analogue: in vitro studies and in vivo preclinical antitumor evaluation in a breast cancer model. *Tumor Biol*. 2015;36(9):7251-7267. doi:10.1007/s13277-015-3441-z.
30. Damião MCFCB, Pasqualoto KFM, Ferreira AK, et al. Novel capsaicin analogues as potential anticancer agents: Synthesis, biological evaluation, and in silico approach. *Arch Pharm (Weinheim)*. 2014;347(12):885-895. doi:10.1002/ardp.201400233.
31. Batista Fernandes T, Alexandre de Azevedo R, Yang R, et al. Arylsulfonylhydrazones induced apoptosis in MDA-MB-231 breast cancer cells. *Lett Drug Des Discov*. 2018;15(1):1-11. doi:10.2174/1570180815666180321161513.
32. Hoeflich KP, Herter S, Tien J, et al. Antitumor efficacy of the novel RAF inhibitor GDC-0879 is predicted by BRAF V600E mutational status and sustained extracellular signal-regulated kinase/mitogen-activated protein kinase pathway suppression. *Cancer Res*. 2009;69(7):3042-3051. doi:10.1158/0008-5472.CAN-08-3563.
33. Davies H, Bignell GR, Cox C, et al. <Davies_2002_Nature_Mutations of the BRAF gene in human cancer.pdf>. 2002:949-954. doi:10.1038/nature00766.
34. Bollag G, Hirth P, Tsai J, et al. Clinical efficacy of a RAF inhibitor needs broad target blockade in BRAF-mutant melanoma. *Nature*. 2010;467(7315):596-599. doi:10.1038/nature09454.
35. Shin MK, Kim JW, Min SK, et al. Associations of the BRAF (V600E) mutation and p53 protein expression with clinicopathological features of papillary thyroid carcinomas patients. *Oncol Lett*. 2015;10(3):1882-1888. doi:10.3892/ol.2015.3401.
36. Holderfield M, Deuker MM, McCormick F, McMahon M. Targeting RAF kinases for cancer therapy: BRAF-mutated melanoma and beyond. *Nat Rev Cancer*. 2014;14(7):455-467. doi:10.1038/nrc3760.

37. Shtivelman E, Davies MA, Hwu P, et al. Pathways and therapeutic targets in melanoma. *Oncotarget*. 2014;5(7):1701-1752. doi:10.18632/oncotarget.1892.
38. Galluzzi L, Bravo-San Pedro JM, Vitale I, et al. Essential versus accessory aspects of cell death: Recommendations of the NCCD 2015. *Cell Death Differ*. 2015;22(1):58-73. doi:10.1038/cdd.2014.137.
39. Elmore S. Apoptosis: A Review of Programmed Cell Death. *Toxicol Pathol*. 2007;35(4):495-516. doi:10.1080/01926230701320337.
40. Eum KH, Lee M. Crosstalk between autophagy and apoptosis in the regulation of paclitaxel-induced cell death in v-Ha-ras-transformed fibroblasts. *Mol Cell Biochem*. 2011;348(1-2):61-68. doi:10.1007/s11010-010-0638-8.
41. Naselli F, Tesoriere L, Caradonna F, et al. Anti-proliferative and pro-apoptotic activity of whole extract and isolated indicaxanthin from *Opuntia ficus-indica* associated with re-activation of the onco-suppressor p16INK4a gene in human colorectal carcinoma (Caco-2) cells. *Biochem Biophys Res Commun*. 2014;450(1):652-658. doi:10.1016/j.bbrc.2014.06.029.
42. Grivicich I, Regner A, da Rocha AB. Morte Celular por Apoptose. *Rev Bras Cancrol*. 2007;53(3):335-343. doi:10.1590/S0102-311X2003000200031.
43. Ferreira AK, Pasqualoto KFM, Krut FAE, et al. BFD-22 a new potential inhibitor of BRAF inhibits the metastasis of B16F10 melanoma cells and simultaneously increased the tumor immunogenicity. *Toxicol Appl Pharmacol*. 2016;295:56-67. doi:10.1016/j.taap.2016.02.008.
44. Adams JM, Cory S. The BCL-2 arbiters of apoptosis and their growing role as cancer targets. *Cell Death Differ*. 2018;25(1):27-36. doi:10.1038/cdd.2017.161.
45. Hata AN, Engelman JA, Faber AC. The BCL2 family: Key mediators of the apoptotic response to targeted anticancer therapeutics. *Cancer Discov*. 2015;5(5):475-487. doi:10.1158/2159-8290.CD-15-0011.
46. Lakhani SA, Masud A, Kuida K, et al. Caspases 3 and 7: Key mediators of mitochondrial events of apoptosis. *Science (80-)*. 2006;311(5762):847-851. doi:10.1126/science.1115035.
47. Hee Oh S, Soon Kim Y, Chul Lim S, Feng Hou Y, Youb Chang I, Jin You H. Dihydrocapsaicin (DHC), a saturated structural analog of capsaicin, induces autophagy in human cancer cells in a catalase-regulated manner. *Autophagy*. 2008;4(8):1009-1019. doi:10.4161/auto.6886.
48. Xue R, Yang J, Wu J, Meng Q, Hao J. Coenzyme Q10 inhibits the activation of pancreatic stellate cells through PI3K/AKT/mTOR signaling pathway. *Oncotarget*. 2017;8(54):92300-92311. doi:10.18632/oncotarget.21247.
49. Yang Y, Guo W, Ma J, et al. Downregulated TRPV1 Expression Contributes to Melanoma Growth via the Calcineurin-ATF3-p53 Pathway. *J Invest Dermatol*. 2018. doi:10.1016/j.jid.2018.03.1510.
50. Alejandro EU, Johnson JD. Inhibition of Raf-1 alters multiple downstream pathways to induce pancreatic cell apoptosis. *J Biol Chem*. 2008;283(4):2407-2417. doi:10.1074/jbc.M703612200.

51. Takaishi M, Uchida K, Suzuki Y, et al. Reciprocal effects of capsaicin and menthol on thermosensation through regulated activities of TRPV1 and TRPM8. *J Physiol Sci.* 2016;66(2):143-155. doi:10.1007/s12576-015-0427-y.
52. Fang JQ, Du JY, Fang JF, et al. Parameter-specific analgesic effects of electroacupuncture mediated by degree of regulation TRPV1 and P2X3 in inflammatory pain in rats. *Life Sci.* 2018;200(September 2017):69-80. doi:10.1016/j.lfs.2018.03.028.
53. Freitas CS, Roveda AC, Truzzi DR, et al. Anti-inflammatory and Anti-nociceptive Activity of Ruthenium Complexes with Isonicotinic and Nicotinic Acids (Niacin) as Ligands. *J Med Chem.* 2015;58(11):4439-4448. doi:10.1021/acs.jmedchem.5b00133.
54. Del Prete D, Caprioglio D, Appendino G, et al. Discovery of non-electrophilic capsaicinoid-type TRPA1 ligands. *Bioorg Med Chem Lett.* 2015;25(5):1009-1011. doi:10.1016/j.bmcl.2015.01.039.
55. Appendino G, Daddario N, Minassi A, Moriello AS, De Petrocellis L, Di Marzo V. The Taming of Capsaicin. Reversal of the Vanilloid Activity of N - Acylvanillamines by Aromatic Iodination. *J Med Chem.* 2005;48(14):4663-4669. doi:10.1021/jm050139q.
56. Jetter MC, Youngman MA, McNally JJ, et al. N-Isoquinolin-5-yl-N'-aralkyl-urea and -amide antagonists of human vanilloid receptor 1. *Bioorg Med Chem Lett.* 2004;14(12):3053-3056. doi:10.1016/j.bmcl.2004.04.038.
57. Smart D, Jerman JC, Gunthorpe MJ, et al. Characterisation using FLIPR of human vanilloid VR1 receptor pharmacology. *Eur J Pharmacol.* 2001;417(1-2):51-58. doi:10.1016/S0014-2999(01)00901-3.
58. Kovacs G, Danko T, Bergeron MJ, et al. Heavy metal cations permeate the TRPV6 epithelial cation channel. *Cell Calcium.* 2011;49(1):43-55. doi:10.1016/j.ceca.2010.11.007.
59. Simonin C, Awale M, Brand M, et al. Optimization of TRPV6 calcium channel inhibitors using a 3D ligand-based virtual screening method. *Angew Chemie - Int Ed.* 2015;54(49):14748-14752. doi:10.1002/anie.201507320.
60. Lee JS, Chang JS, Lee JY, Kim JA. Capsaicin-induced apoptosis and reduced release of reactive oxygen species in MBT-2 murine bladder tumor cells. *Arch Pharm Res.* 2004;27(11):1147-1153. doi:10.1007/BF02975121.
61. Death CC, Ramírez-barrantes R, Córdova C, et al. Transient Receptor Potential Vanilloid 1 Expression Mediates. 2018;9(June):1-10. doi:10.3389/fphys.2018.00682.
62. Liao M, Cao E, Julius D, Cheng Y. Structure of the TRPV1 ion channel determined by electron cryo-microscopy. *Nature.* 2013;504(7478):107-112. doi:10.1038/nature12822.
63. Caterina MJ, Schumacher MA, Tominaga M, Rosen TA, Levine JD, Julius D. The capsaicin receptor: A heat-activated ion channel in the pain pathway. *Nature.* 1997;389(6653):816-824. doi:10.1038/39807.
64. Faidallah HM, Al-Mohammadi MM, Alamry KA, Khan KA. Synthesis and

- biological evaluation of fluoropyrazolesulfonylurea and thiourea derivatives as possible antidiabetic agents. *J Enzyme Inhib Med Chem*. 2016;31(May):157-163. doi:10.1080/14756366.2016.1180594.
65. Clark DE. Rapid calculation of polar molecular surface area and its application to the prediction of transport phenomena. 1. Prediction of intestinal absorption. *J Pharm Sci*. 1999;88(8):807-814. doi:10.1021/js9804011.
 66. Mignani S, Rodrigues J, Tomas H, et al. Present drug-likeness filters in medicinal chemistry during the hit and lead optimization process: how far can they be simplified? *Drug Discov Today*. 2018;23(3):605-615. doi:10.1016/j.drudis.2018.01.010.
 67. Varentsov VK, Koshev AN, Sukhov IF. Mathematical Modeling and Experimental Studies of the Joint Electrodeposition of Gold and Silver from Sulfuric Acid Thiourea Solutions on Flow-Through 3D Electrode Taking into Account Its Nonstationary State. *Theor Found Chem Eng*. 2018;52(4):495-505. doi:10.1134/S004057951803017X.
 68. Linke P, Amaning K, Maschberger M, et al. An Automated Microscale Thermophoresis Screening Approach for Fragment-Based Lead Discovery. *J Biomol Screen*. 2016;21(4):414-421. doi:10.1177/1087057115618347.
 69. Mosmann T. Rapid colorimetric assay for cellular growth and survival: Application to proliferation and cytotoxicity assays. *J Immunol Methods*. 1983;65(1-2):55-63. doi:10.1016/0022-1759(83)90303-4.
 70. Kovacs G, Montalbetti N, Simonin A, et al. Inhibition of the human epithelial calcium channel TRPV6 by 2-aminoethoxydiphenyl borate (2-APB). *Cell Calcium*. 2012;52(6):468-480. doi:10.1016/j.ceca.2012.08.005.
 71. Zimmermann M. Ethical guidelines for investigations of experimental pain in conscious animals. *Pain*. 1983;16(2):109-110.
 72. Snedecor, G. W; Sokal, R.R; Rohlf FJ. *Statistical Methods Biometry*. 4th ed. (Ames, ed.). New York; 1946.
 73. Sokal, R. R; Rohlf FJ. *Biometry*. (Co WHF, ed.). New York; 1981.
 74. Korb O, Monecke P, Hessler G, Stützle T, Exner TE. pharmACOPhore: Multiple Flexible Ligand Alignment Based on Ant Colony Optimization. *J Chem Inf Model*. 2010;50(9):1669-1681. doi:10.1021/ci1000218.
 75. Vainio MJ, Puranen JS, Johnson MS. ShaEP: Molecular Overlay Based on Shape and Electrostatic Potential. *J Chem Inf Model*. 2009;49(2):492-502. doi:10.1021/ci800315d.
 76. Trott O, Olson AJ. AutoDock Vina: Improving the speed and accuracy of docking with a new scoring function, efficient optimization, and multithreading. *J Comput Chem*. 2010;31(2):455-461. doi:10.1002/jcc.21334.